ACTIVITY REPORT

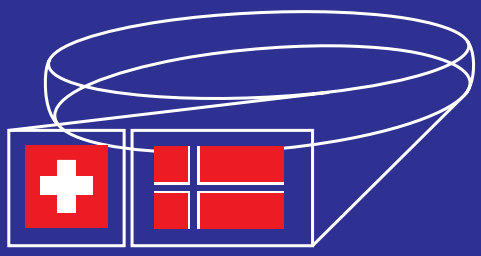

Swiss-Norwegian Beam Lines
at ESRF

SNBL

07/08

07/08

ACTIVITY REPORT

CONTENTS

In addition to the routine operation of the beamlines, the last two years have seen two events which will have a serious impact on the future development of the Swiss-Norwegian beamline project. On the one hand, we have successfully completed a major upgrade of the entire infrastructure of the beamlines (including electrical, mechanical and vacuum systems). Although this upgrade has taken somewhat longer than originally planned, we are particularly pleased to be able to report that the entire refurbishment was carried out without any significant impact on our day-to-day operations. We are now in excellent shape to continue to offer high grade synchrotron facilities to our user communities in Norway and Switzerland for many years to come.

The second major event was the review of SNBL carried out by an international committee of experts nominated by the ESRF, which takes place roughly every 5 years. This review provides us with an excellent opportunity both to present our achievements over the past few years and to look forward to the possibilities and the challenges which lie ahead. We would like to acknowledge the very positive and constructive atmosphere in which the review was conducted, and the interest shown by the panel members. Although the results of the review are considered in detail within this bi-annual report, we would like to take this opportunity to quote from the main conclusions of the review panel.

"*The Panel was impressed by the high quality and quantity of science as well as technical achievement since the last review. We formed the view that the activities at the SNBL are strongly science-driven and supported by an excellent well-motivated staff who are delivering a cohesive portfolio of techniques from the two member nations. BM01 operates as an important interface between the various ESRF operations, offering state-of-the-art experimental facilities and data analysis for the chemistry community and more generally across the physical science*".

To receive such positive feed-back from the review panel has been both a source of encouragement for all members of the team, and a confirmation that the management of the SNBL (in conjunction with the members of the SNX Council and the user community) has adopted the right strategy for the future development of the project. In this context, it is perhaps appropriate to cite the final remarks of the review panel.

"*The beamline has a very bright scientific future building upon the impressive output to date and unique features of the beamline*".

V. DMITRIEV, P. PATTISON, H. EMERICH

SCIENTIFIC HIGHLIGHTS

Structural Studies of Peroxide-Derived Myoglobin Intermediates.

Hans-Petter Hersleth and K. Kristoffer Andersson
University of Oslo, Department of Molecular Biosciences, P.O. Box 1041 Blindern, N-0316 Oslo, Norway

The main function of myoglobin (Mb) is oxygen storage and transportation in heart and skeletal muscle. However, Mb exhibit peroxidase-activity during oxidative stress with involvement in scavenging of reactive oxygen species or oxidising lipids. When Mb reacts with peroxides it goes through similar intermediates as found in peroxidases and oxygenases. Our interest is concentrated around the peroxidase function of Mb to gain further knowledge of this process and its intermediates. A summary of the reactions we have been studying with protein crystallography are described in the reaction scheme *Scheme 1*.

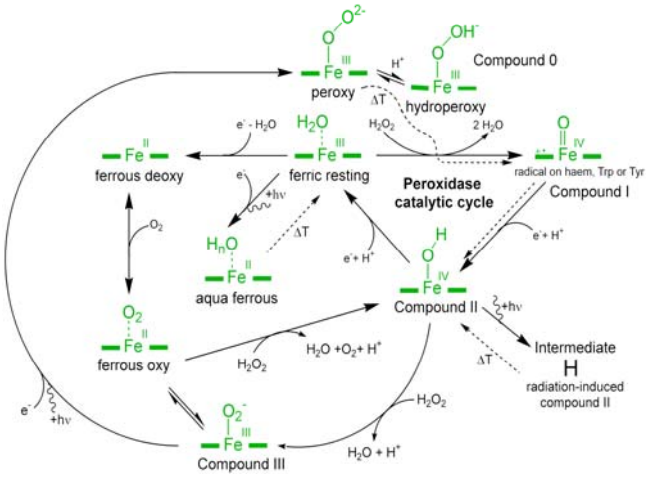

Scheme 1: Reaction cycle studied in Mb

Radiation damage

In recent years the awareness of potential radiation damage of metal centres in protein crystals during crystallographic data collection has received increasing attention. The radiation damage can lead to radiation-induced changes and reduction of the metal sites. For our studies on Mb we have observed this, and have therefore regularly used microspectrophotometry to monitor the influence of X-ray on our different states during X-ray diffraction data collection. Mb can nicely be monitored with light absorption because the different Mb states have characteristic absorptions in the 350-700 nm range. We have mainly studied three of the Mb states: resting ferric metMb, Mb compound II, Mb compound III and their corresponding radiation-induced states.

Radiation-induced resting ferric metMb

The ferric metMb is the resting state in the peroxidase reaction of Mb, and due to its ferric oxidation state it can potentially be reduced. This undesired radiation-induced change is observed for the ferric metMb state during crystallographic data collection. The radiation-induced reduction reduces the Fe^{III} to Fe^{II}, but at this low temperature the water that ligates to the iron is unable to move away to generate the normal ferrous deoxy. The crystal structure of the aqua ferrous low-spin state can be seen in *Fig. 1A* with a Fe-O bond of 2.1 Å, which is about 0.1 Å shorter than in the high-spin ferric metMb state. The

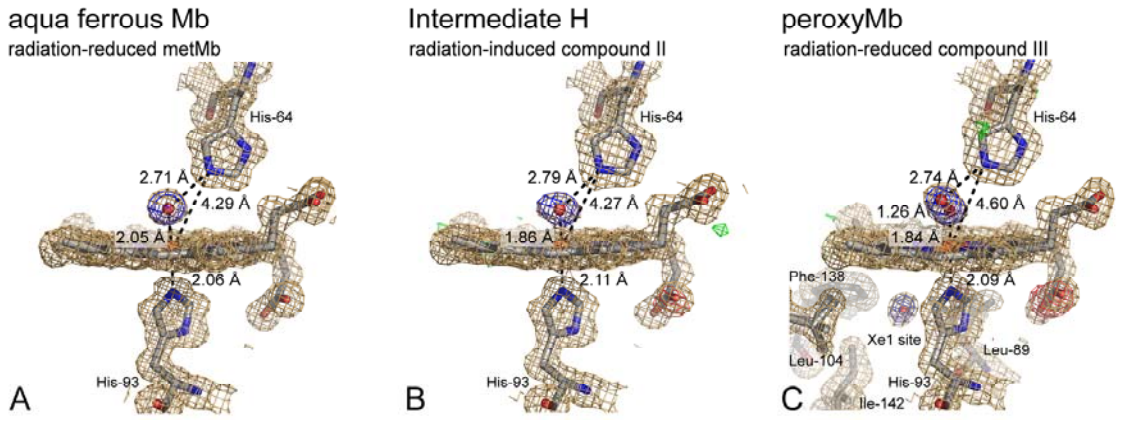

Figure 1: The Crystal structures of the haem regions

cryoradiolytic-induced conversion from ferric metMb to aqua/hydroxy-ferrous Mb can in crystals be followed with single-crystal microspectrophotometry as seen in *Fig. 2*. The reduction is characterised by the reduction of the original ferric metMb peaks at 500, 540, 580 and 635 nm, with new peaks at 525 and 567 nm. When we carry out a short annealing of the aqua-ferrous state in crystals it seems that it is the high-spin ferric Mb state that is regenerated and not the ferrous deoxy state *(Fig. 2)*.

Radiation-induced Mb compound II

Single-crystal microspectrophotometry on Mb compound II shows radiation-induced changes during crystallographic data collection. The peaks at 540 and 580 as well as the shoulder peak at 595 nm decreases with increasing dose, while a new peak at 567 nm of unknown origin appears. The structure of this radiation-induced Mb compound II has a Fe-O bond of 1.85-1.90 Å, which indicate a single-bond *(Fig. 1B)*. The observation of a single-bond in compound II is supported by crystallographic studies on peroxidases. Fe-O bond distance of 1.85-1.90 Å is about 0.3 Å longer than expected for an oxoferryl (Fe^{IV}=O) species and about 0.2 Å shorter than in the radiation-induced ferric Mb structures. We have also collected datasets with shorter exposure time, and only partially radiation-induced structures as shown from single-crystal light absorption spectra. These structures show similar Fe-O bond distances of 1.85-1.90, which indicates that the unaffected compound II and the radiation-induced compound II may have similar structures. Quantum refinement showed that at least in the radiation-induced Mb compound II crystal structure, the oxygen atom bound to the iron is protonated (Fe-OH). We believe, as mentioned above, that the structure of the Mb compound II and radiation-induced Mb compound II are similar, and thereby both Fe-OH states. Due to the shown protonation of the radiation-induced Mb compound II it has also been referred to as Mb intermediate H.

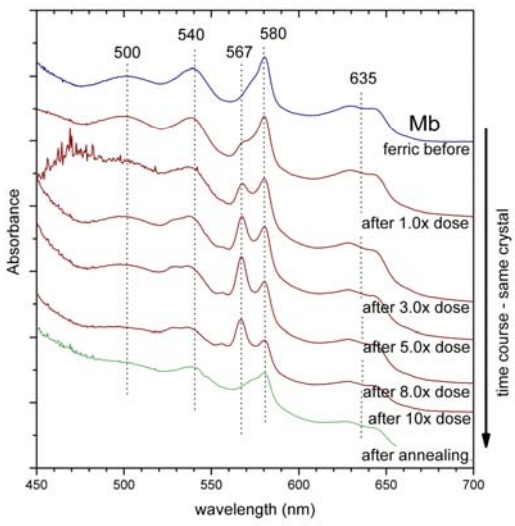

Figure 2: Single crystal-light absorption spectra of the Build up of aqua ferrous Mb from ferric Mb during increased X-ray dose.

Radiation-induced generation of peroxyMb from Mb compound III

Mb compound III, which is similar to a ferrous-oxy (or ferric-superoxy) state (*Scheme 1*) has been generated in Mb crystals *(Fig. 1C)*. As with the other Mb states, Mb compound III also experiences a fast one-electron reduction by the synchrotron radiation during the crystallographic data collection. A one-electron reduction of the compound III leads to a peroxy intermediate that is isoelectronic with compound 0. The formation of compound III from compound II in Mb crystals can be seen by the disappearance of the 595 nm light absorption shoulder peak, resulting in only two quite sharp peaks at 540 and 580 nm *(Fig. 3)*. This is typical for low-temperature oxyMb spectra. The Mb compound III peaks at 540 and 580 nm decrease, while a new small peak at 567 nm appears showing the formation of peroxyMb *(Fig. 3)*. The peroxyMb structure have O-O bonds of ~1.3 Å and Fe-O distance of ~1.8-1.9 Å. The overall structure is quite similar to both radiation-induced ferric Mb and radiation-induced Mb compound II structures *(Fig 1)*. Quantum refinement on peroxyMb generated from compound III shows that the major unpaired spin density resides on the O-O, indicating a Fe^{II}-O-O^{-}, superoxy state.

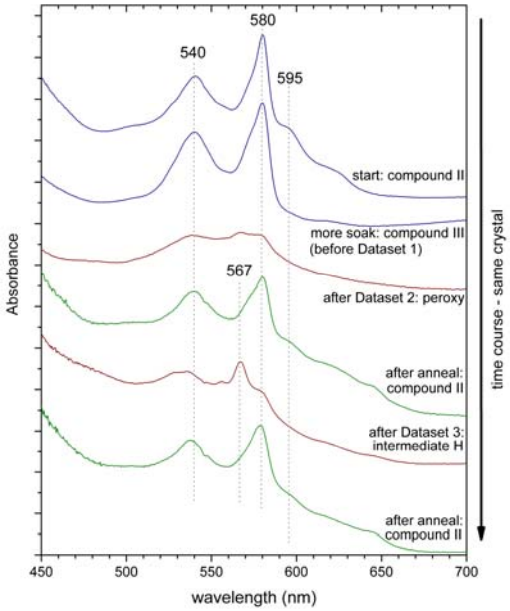

Figure 3: Single crystal-light absorption spectra to monitor the changes experiences by the crystal subjected to collection of Datasets 1, 2 and 3.

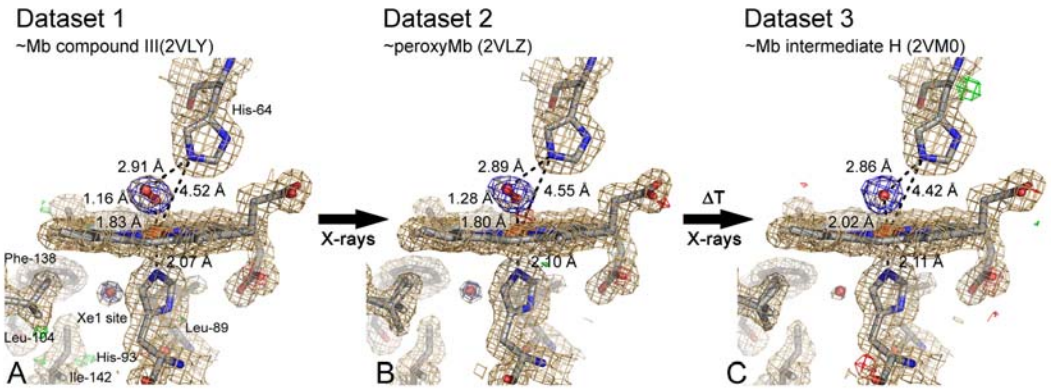

Figure 4: Crystal structures of the haem regions of Mb shown with the electron density $2F_o$-F_c map (contoured at 1σ in golden), the final F_o-F_c map (at +3σ in green and at -3σ in red) and difference F_o-F_c map with the peroxy/hydroxy atoms and extra water molecule omitted for map calculation (at 4σ in blue). Consecutive datasets collected on the same crystal.

Consecutive datasets and breaking of the oxygen-oxygen bond

We have collected two consecutive datasets on a Mb compound III crystal, the first one with a dose of ~3 MGy (Dataset 1), and the second one with a dose of ~10 MGy (Dataset 2). The light absorption spectrum collected after Dataset 2 shows the characteristic

peroxyMb features *(Fig. 3)*. The structures resulting from Dataset 1 and Dataset 2 are shown in *Fig. 4A and 4B*, and indicate a shorter O-O bond for the former. The trend indicates that Dataset 1 is mostly compound III (oxy) with a shorter O-O bond, while Dataset 2 is mostly peroxyMb, but the resolution is not high enough to give conclusive results. A short annealing of 1 sec. of the peroxyMb crystal (Dataset 2) resulted in the formation of Mb compound II *(Fig. 3, after annealing)*. The characteristic shoulder at 595 nm can be seen, but it has a relative lower intensity than normal, so the conversion might not be complete. The structure of the dataset collected on this state (Dataset 3) can be seen in *Fig. 4C*, and will during data collection result in the radiation-induced compound II as indicated by the light absorption spectra *(Fig. 3)*. From *Fig. 4B and 4C* it is clearly seen by the electron density difference maps that the molecular oxygen has changed into a single oxygen atom. These results show that compound III can be cryoradiolytically reduced to a peroxyMb state that after protonation is analogous to the proposed compound 0 precursor in the reaction with hydrogen peroxide.

Summary

The structural studies on Mb have shown that most oxidised states of Mb experience some radiation-induced changes during crystallographic data collection from interactions with X-rays, and similar observations have been made for other haem proteins. The ferric metMb, Mb compound II and Mb compound III experiences undesired X-ray radiation-induced changes/reductions. The X-ray induced reduction during crystallographic data collection can also be used to add an electron to a state at low temperatures, generating intermediates that are otherwise unattainable. For Mb the crystal structure of peroxyMb has been generated in this way from Mb compound III. An annealing of the peroxyMb has shown that the oxygen-oxygen bond is broken in the crystal resulting in Mb compound II. This shows a way of trapping such intermediates, and that the peroxy/hydroperoxy state is an important intermediate in Mb peroxidase reaction cycle.

Acknowledgements

Our investigation has been supported by funding from the Norwegian Research Council: grant 177661/V30 (to K.K.A) and grant 138370/V30 (Synchrotron related research in the Oslo-region, SYGOR).The team at the Swiss-Norwegian Beam Line (BM01) is thanked for their valuable help.

Publications:

1. Hersleth, H.-P., Hsiao, Y.-W., Ryde, U., Görbitz, C.H. & Andersson, K.K. (2008) The crystal structure of peroxymyoglobin generated through cryoradiolytic reduction of myoglobin compound III during data collection. *Biochem. J*. 412, 257-264

2. Hersleth, H.-P., Uchida, T., Røhr. A.K., Teschner, T., Schünemann, V., Kitagawa, T., Trautwein, A.X., Görbitz, C.H. & Andersson, K.K. (2007) Crystallographic and Spectroscopic Studies of Peroxide-Derived Myoglobin Compound II and Occurrence of Protonated Fe^{IV}-O. *J. Biol. Chem.* 282, 23372-23386.

3. Hersleth, H.-P., Ryde, U., Rydberg, P., Görbitz, C.H., Andersson, K.K. (2006) Structures of the high-valent metal-ion haem-oxygen intermediates in peroxidases, oxygenases and catalases. *J. Inorg. Biochem*. 100, 460-476.

4. Hersleth, H.-P., Varnier, A., Harbitz, E., Røhr, Å.K., Schmidt, P. P., Sørlie, M., Cederkvist, F.H., Marchal, S., Gorren, A.C.F., Mayer, B., Uchida, T., Schünemann, V., Kitagawa, T., Trautwein, A.X., Shimizu, T., Lange, R., Görbitz, C.H. & Andersson, K.K. (2008) Reactive complexes in myoglobin and nitric oxide synthase. *Inorg. Chim. Acta* 361, 831-843.

5. Hersleth, H.-P., Hsiao, Y.-W., Ryde, U., Görbitz, C.H. & Andersson, K.K. (2008) The Influence of X-Rays on the Structural Studies of Peroxide-Derived Myoglobin Intermediates. *Chem. Biodiv.* In press.

Structure of the polycrystalline zeolite catalysts solved by enhanced charge flipping

Christian Baerlocher and Lynne McCusker
ETH Zürich, Switzerland

A research team from the Laboratory of Crystallography of ETH Zurich has succeeded in solving the structure of the zeolite IM-5, which was first synthesized about ten years ago. However its makeup is so complex that its structure could not be clarified until now. This was mainly because IM-5 is available only in powder form. All that researchers were able to infer from catalytic test reactions in 2000 was a rough picture of IM-5's pore system. The present studies show that IM-5 has a basic structure of 24 individual silicon atoms. A unit cell of the crystal consists of 864 atoms. However, because of various symmetries, "only" over 70 atomic positions needed to be determined. It should be stressed that up to now the upper limit for polycrystalline materials was 20 to 30 atoms. In the present case the structure is more than twice as big. This means the structure of IM-5 is as complex as that of the zeolite TNU-9. So far the latter has been the most complex structure that the same ETH Zurich research group was also able to solve.

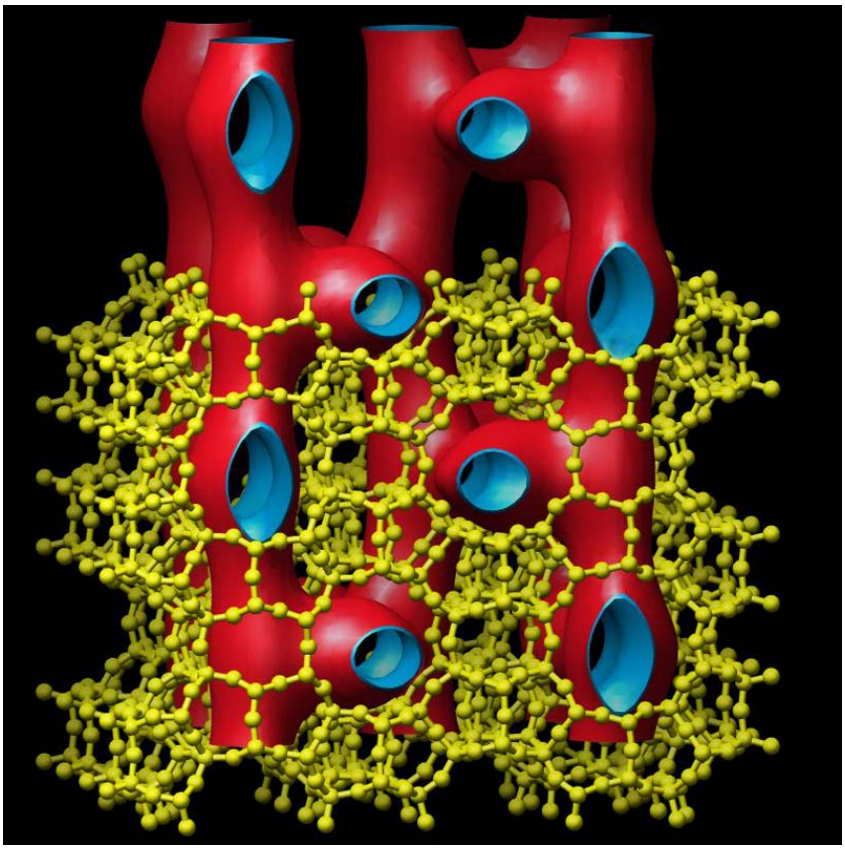

Fig. 1 A model representation of the zeolite IM-5: the yellow skeleton outlines the position of the silicon-oxygen atoms and the red-blue tubes illustrate the unique pore system

One of IM-5's special features is its unusual pore and channel system. On the one hand this is two-dimensional, i.e. it has countless channels running in parallel, but on the other hand it has limited three-dimensionality as a result of cross-links between the parallel pores and dead end side-branches. Groups of three pore systems lying in a plane are interconnected. These nano-sized planes are separated by single walls. The team from the ETHZ and their colleagues from Stockholm University broke new ground to solve the structure. The structural determination was based on data from X-ray powder diffraction experiments collected at SNBL and at the Swiss Light Source, together with high resolution electron transmission microscopy images and a computer model ("Charge Flipping") which they adapted to the specific needs in determining the complex crystal structures of powders.

The use of the charge flipping algorithm for *ab initio* structure solution from single crystal data has rapidly become well-established, and is now incorporated into a number of different software packages. Amongst other examples, data was presented from SNBL on a zeolite ZSM-5 containing 38 atoms in the asymmetric unit.

In the case of the high-silica zeolite catalyst SSZ-74, it was indeed possible to obtain a high resolution TEM image (albeit only in one direction). This restriction meant that the phase information which could be extracted from the HRTEM image was very limited. Nevertheless, it was possible to use the image to construct a structure envelope for this zeolite, which could then be combined with the charge flipping procedure. After a series of cycles of phasing and inspection of the density maps, a fully connected atomic framework could be recognized.

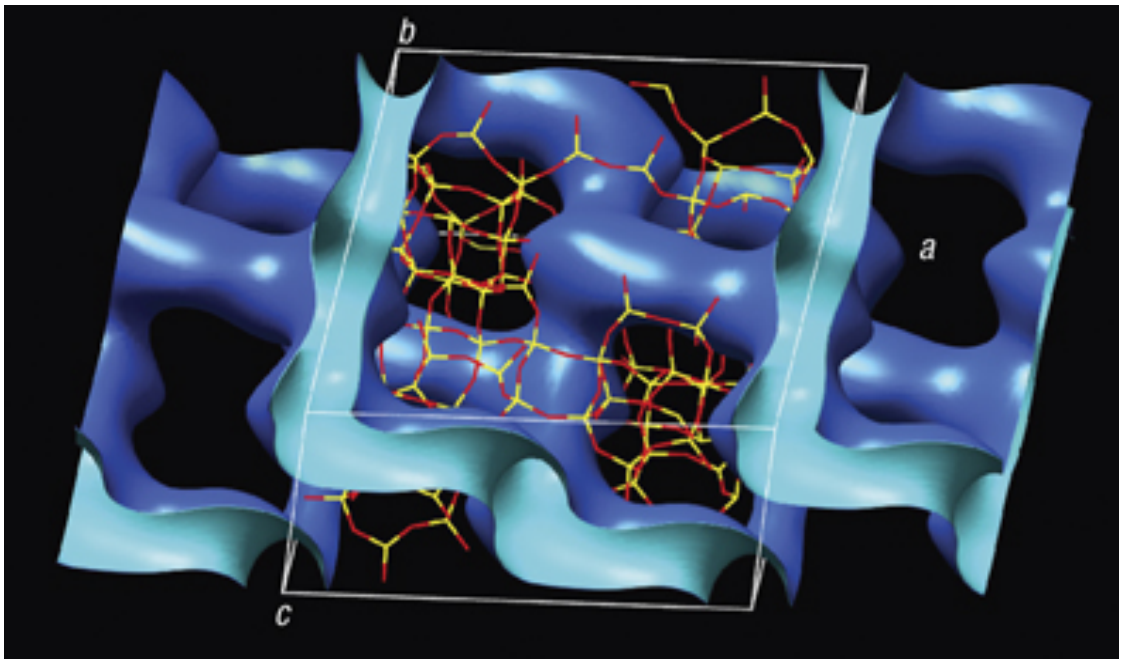

Fig. 2 The framework structure and channel system of SSZ-74. Si:yellow, O:red. The periodic nodal surface depicts approximately the channel system within the framework structure.

The original powder data collected at Brookhaven turned out to be of insufficient quality to proceed with a structure refinement, and therefore new data were collected at SNBL. The new powder data allowed not only 23 of the expected 24 Si atoms to be identified, but it was also possible to demonstrate conclusively that the missing Si atom was in fact an ordered vacancy. Such an ordered defect, with four framework oxygen atoms forming an approximate tetrahedron around a vacancy, has never been observed before in a high-silica zeolite.

The key to the structure determination of this complex zeolite has proved to be the combination of powder diffraction and electron microscopy data within the charge-flipping algorithm. Not only could 89 atoms (23Si + 48O + 16C + 2N) in the asymmetric unit be located, but even the totally unexpected Si vacancy was revealed. This approach to structure determination is widely applicable, and therefore holds much promise for those polycrystalline materials which have hitherto resisted solution.

Publications:

Christian Baerlocher, Fabian Gramm, Lars Massüger, Lynne B. McCusker, Zhanbing He, Sven Hovmöller, and Xiaodong Zou *Science* **315** , 1113-1116 (2007)
Christian Baerlocher, Lynne B. McCusker and Lukas Palatinus *Z. Kristallographie* **222**, 47-53 (2007)
Christian Baerlocher, Dan Xie, Lynne B. McCusker, Song-jong Hwang, Ignatius Y. Chan, Kenneth Ong, Allen W. Burton and Stacey I. Zones *Nature Materials*, **7** 631-635 (2008)

Structural studies of novel materials for hydrogen storage

Bjørn C. Hauback and Magnus H. Sørby
Physics Department, Institute for Energy Technology (IFE), Norway

During the last decade there has been a significantly increased focus on hydrogen as the future energy carrier. The main reason is that a hydrogen economy may be an answer to the two major challenges facing the future global economy: climate changes and the security of energy supplies. The major components in the expected Hydrogen Economy involve production, storage and final use of hydrogen, e.g. in fuel cells. All parts in this chain are facing considerable technological challenges, in particular related to the key materials. Hydrogen storage is a crucial step for providing a ready supply of hydrogen fuel to an end user, such as in a car. Hydrogen storage remains an undisputed problem for hydrogen-fuelled vehicles, and it is considered by many to be the most technologically challenging aspect. It is also clear that the only acceptable sustainable long-term solution for vehicles is hydrogen storage in solid materials.

A major challenge is to find materials and hydrogen storage systems fulfilling international targets for hydrogen storage. Such research efforts require new materials and not simple, incremental improvements in current technologies. One of the main goals is related to the overall weight of the storage system, and thus the hydrogen storage materials should be based on light-weight elements in the Period Table. During the last years several new metal hydrides based on boron, aluminium, magnesium and nitrogen have been synthesized. Advanced characterization tools like synchrotron X-ray diffraction have to be used in order to for determination of:

- Crystal structure of the hydride and also intermediate phases that can be present during hydrogen absorption/desorption. For structural determination of hydrogen storage materials the combination of synchrotron powder X-rays (SR-PXD) and powder neutron diffraction (PND) is very important (details about hydrogen/deuterium positions from neutrons and heavier elements from X-rays)
- Hydrogen desorption and absorption reactions. The process for hydrogen absorption and desorption in many of the new light-weight hydrides can be very complex involving several steps and intermediate phases. *In-situ* SR-PXD experiments are important for detailed understanding of theses sorption processes.
- Effect of catalysts in novel complex hydrides. Catalysts are crucial for better kinetics in these compounds. However, the understanding of the effect of the catalysts in these compounds is still limited, and the use of SR-PXD in combination with for example TEM and spectroscopic techniques, contributes to a better understanding.

In the period 2005-2007 we have used both the A and B stations on BM01 at ESRF (SNBL) to investigate:

- Crystal structures for several new compounds (in combination with PND at IFE) including: $Mg(AlH_4)_2$, Na_2LiAlD_6, $Zr_2NiD_{4.5}$, α'-, β- and γ-AlD_3, $LiMg(AlD_4)_3$, $LiMgAlD_6$, $LiND_2$ and $Mg(ND_2)_2$.
- Detailed studies of desorption processes in different compounds based on Al ($Mg(AlH_4)_2$, $LiAlH_4$, α'-, β- and γ-AlD_3, $LiMg(AlD_4)_3$), N (Li-Mg-N-H systems), Mg (Mg-Co-H, Mg-Fe-H, Mg-Ti-Ni-H) and B ($Ca(BH_4)_2$, $Mg(BH_4)_2$).
- Details of effect of transition metal (TM) catalysts in $NaAlH_4$ including presence of TM-Al solid solutions and amorphous phases (in combination with high resolution TEM and PND).

- Substitution of fluorine for hydrogen in Na_3AlH_6 in order alter the stability.

In the following one example describing structure and decomposition of the different phases of AlH_3 and decomposition of the B-containing complex hydrides $Ca(BH_4)_2$ and $Mg(BH_4)_2$ will be presented.

Structural studies and decomposition of AlH_3

Aluminium hydride AlH_3 (alane) has both a high hydrogen content (10.1 wt%) and volumetric density (0.148 kg H_2/L) that can be released at moderate temperatures. However, the compound is not reversible at moderate conditions. AlH_3 has been found to take at least six different crystal structures depending on the synthesis route: α, α', β, γ, δ and ε. α-AlH_3 was the only structure known before this work. Based on SR-PXD experiments at SNBL (BM01B) in combination with PND the accurate structures of α'-, β- and γ-AlD_3 in addition to α-AlD_3 have been determined [1-3]. The structures of the different structures consisting AlD_6 octahedra are shown in Figure 1. For the α-, α'- and β modifications the octahedra are connected via corner-sharing in different ways, but for the γ-AlD_3 the structure consists of both corner- and edge-sharing AlD_6 octahedra.

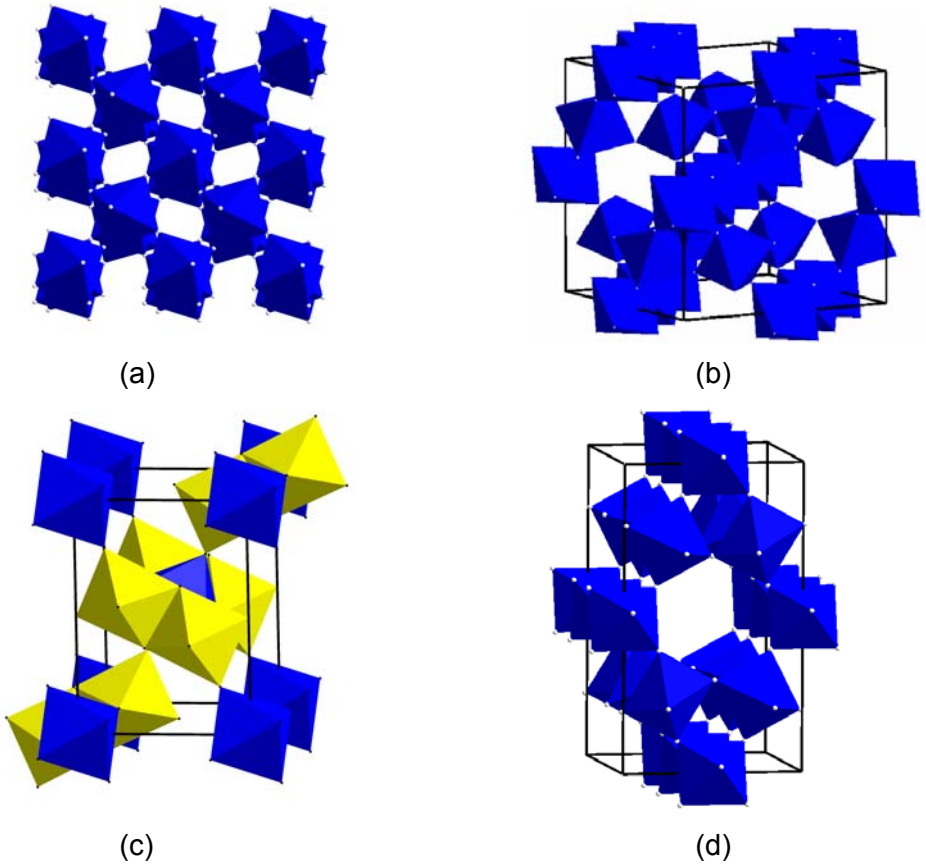

Figure 1. Structures of different modifications of AlD_3: (a) α-AlD_3; (b) α'-AlD_3; (c) β-AlD_3 and (d) γ-AlD_3.

From old work it has been reported that the α polymorph is the most stable, but modelling work has shown that the β-state is more stable than the α-phase. To clarify these points, we have performed detailed studies of the decomposition of α'-, β- and γ-AlD_3 at BM01A [4-5]. The β-AlD_3 transforms into α-AlD_3 (starts at about 80 °C) prior to decomposition to Al and D_2. The transformation of γ-AlD_3 into α-AlD_3 starts at about 90 °C and the sample decomposes to Al and D_2 at a higher temperature. From about 110 °C γ-AlD_3 also decomposes directly into Al and D_2. Relative amounts of the different phases developed as a function of temperature during decomposition of β- and γ-AlD_3, respectively, are shown in Figure 2.

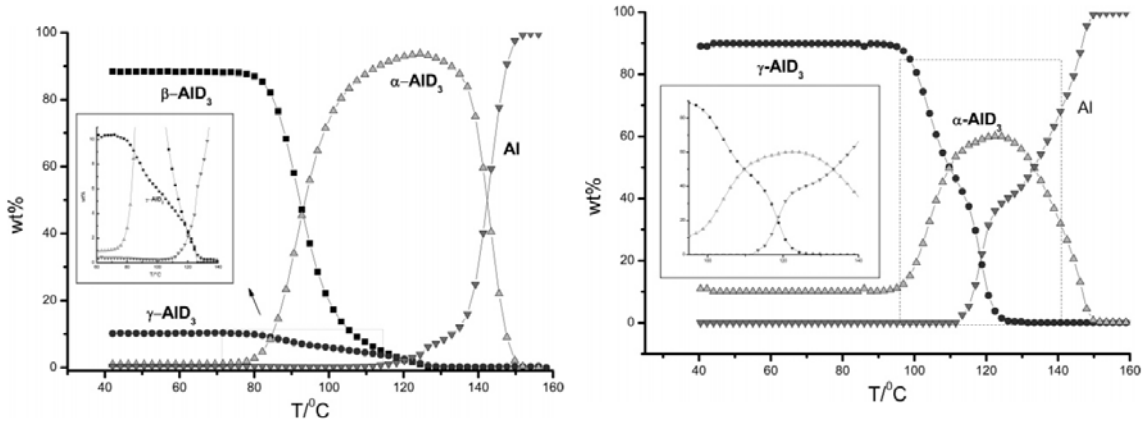

(a) (b)

Figure 2. In-situ SR-PXD studies of the decomposition of: (a) β-AlD_3 and (b) γ-AlD_3 as a function of temperature. Heating rate is 1 K/min and measurements are performed every 2nd minute. The relative amounts of the different compounds were determined by quantitative phase analysis using the Rietveld method based on the SR-PXD data.

From similar analysis we have found that α'-AlD_3 transforms directly into Al and D_2 at around 80 °C [5]. At higher temperatures the transformation of α'-AlD_3 to α-AlD_3 was observed.

In-situ SR-PXD studies of phase transformation and thermal decomposition of $Mg(BH_4)_2$ and $Ca(BH_4)_2$

$Mg(BH_4)_2$ and $Ca(BH_4)_2$ with 14.9 and 11.6 wt% hydrogen, respectively, are among the most promising materials for mobile hydrogen storage, but the knowledge about their hydrogen desorption properties is limited. We have studied these materials by time-resolved *in-situ* SR-PXD at BM01A [6].

For $Mg(BH_4)_2$ system the phase transition from the α- to the β-modification is observed in the temperature range 450-460 K and the decomposition of the β-modification takes place between 520 and 580 K. After decomposition Mg, MgO, and, at higher temperatures, MgH_2 are identified as product phases.

The phase transitions and thermal decomposition of $Ca(BH_4)_2$ are very complex. We have found: (i) a continuous phase transition from the low temperature γ- to the high temperature β-$Ca(BH_4)_2$ and thereafter to "δ-$Ca(BH_4)_2$"; (ii) release of hydrogen in 2 steps (decomposition of β-$Ca(BH_4)_2$ and "δ-$Ca(BH_4)_2$", respectively; (iii) CaH_2 present at 770 K. More work is needed to clarify the structural details for the different $Ca(BH_4)_2$ phases.

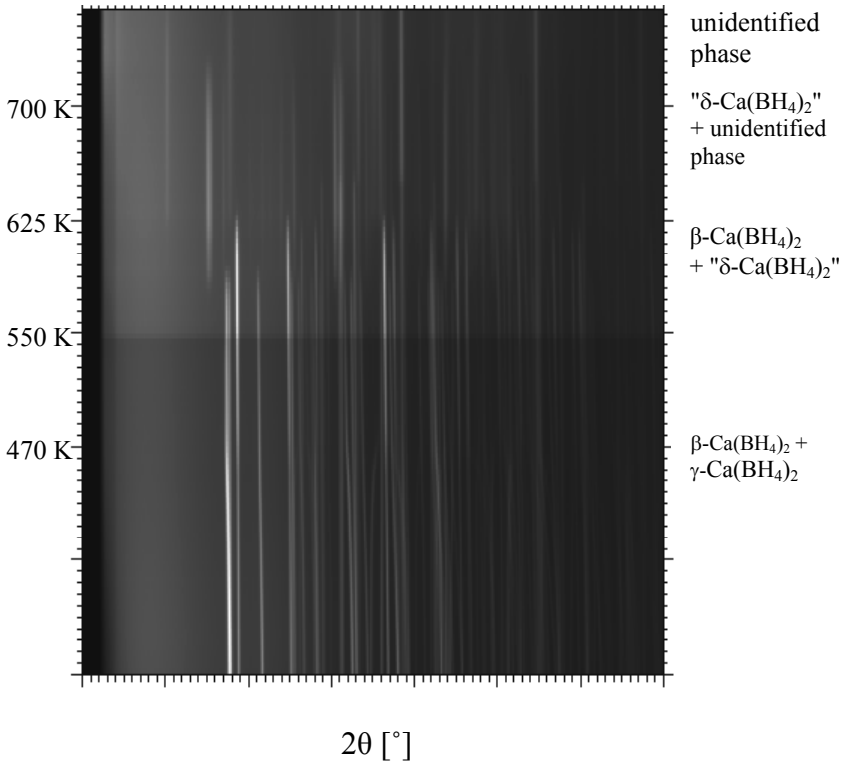

Figure 3. SR-PXD patters for $Ca(BH_4)_2$ as a function of temperature (310-770 K).

Publications

1. H. W. Brinks, A. Istad-Lem, B. C. Hauback, Mechanochemical synthesis and crystal structure of α'AlD_3 and α-AlD_3. *J. Phys. Chem. B* **110** (2006) 25833-25837.
2. H. W. Brinks, W. Langley, C. M. Jensen, J. Graetz, J. J. Reilly, B. C. Hauback, Synthesis and crystal structure of β-AlD_3. *J. Alloys Compd.* **433** (2007) 180-183.
3. H. W. Brinks, C. Brown, C. M. Jensen, J. Graetz, J. J. Reilly, B. C. Hauback, The crystal structure of γ-AlD_3. *J. Alloys Compd.* **441** (2007) 364-367.
4. H. Grove, M. H. Sørby, H. W. Brinks, B. C. Hauback, In situ synchrotron powder X-ray diffraction studies of the thermal decomposition of β- and γ-AlD_3. *J. Phys. C* **111** (2007) 16693-16699.
5. S. Sartori, S. M. Opalka, O. M. Løvvik, M. N. Guzik, X. Tang, B. C. Hauback, Experimental studies of α-AlD_3 and α'-AlD_3 versus first-principles modelling of the alane isomorphs. *J. Mater. Chem.* **18** (2008) 2361-2370.
6. M. D. Riktor, M. H. Sørby, K. Chłopek, M. Fichtner, F. Buchter, A. Züttel, B. C. Hauback, *In situ* synchrotron diffraction studies of phase transitions and thermal decomposition of $Mg(BH_4)_2$ and $Ca(BH_4)_2$. *J. Mater. Chem.* **17** (2007) 4939-4942.

Synthesis and transformation of nanomaterials studied by *in situ* powder diffraction

Heidi Ø. Nielsen, Tao Gao, Rune E. Johnsen, Helmer Fjellvåg, and Poul Norby

Department of Chemistry and Center for Materials Science and Nanotechnology, University of Oslo, P.O. Box 1033, Blindern, N-0315 Oslo, Norway

In order to obtain an improved understanding of the formation/synthesis and transformation of nanomaterials, we have undertaken a number of *in situ* studies using synchrotron X-ray powder diffraction. We are especially interested in size and morphology control in synthesis of nanocrystals and nanostructures.

In connection with establishment of a Centre for Resaerch Based Innovation in Norway (led by the University of Oslo) inGAP (Innovative Natural Gas Reactions and Processes), we have built up a system for studies of catalytic materials under operative conditions at SNBL. The system allows studies of materials under flow conditions with pressures up to 20 atm. to be performed while studying the exhaust gas composition using a mass spectrometer. Together with the *in situ* Raman spectrometer available at SNBL, we have a powerful and unique tool for studies of materials under a wide variety of chemical conditions. The gas system will be described in detail elsewhere.
Here we intend to give a few examples of *in situ* studies of synthesis and transformation of nanomaterials and nanostructures.

Hydrothermal synthesis of Co_3O_4 nanocubes[1].

Co_3O_4 is a promising material for use in e.g. gas sensors, pigments, catalysis, electrochemistry, magnetism, energy storage etc. We aim at synthesizing Co_3O_4 nanocubes for use in different applications in nanodevices. The nanocrystals may for example be of interest for use in core-shell materials. For this purpose, the nanoparticles should be free standing, monodisperse, have a well defined morphology and small size distribution[1,2].

A hydrothermal synthesis route for preparation of well-facetted Co_3O_4 nanocrystals has been developed in the research group [3]. These syntheses typically yield nanocrystals from 10 – 90 nm, and the crystals tend to agglomerate. An alternative hydrothermal approach utilizing micro waves for heating has been successfully explored[1], which gives a smaller size distribution (10 – 20 nm). A reflux method developed by Xu *et al*.[4] using a surfactant, Tween-85, also yields well-facetted Co_3O_4 crystals, with a very narrow size distribution.

The hydrothermal formation of Co_3O_4 nanocubes was studied using *in situ* synchrotron X-ray powder diffraction in order to obtain information on the formation mechanism of the nanocrystals. Our emphasis has been on investigating the intermediate phases and crystallite size as a function of time or temperature. We have also briefly started to explore the reaction kinetics, revealing crystallization mechanisms.

In a typical synthesis, 0.00125 mmol of $Co(NO_3)_2 \cdot 6H_2O$ (98 %, Merck) and 0.0176 mmol $NaNO_3$ (>99.0%, J.T. Baker) was dissolved in 12.5 mL ion exchanged water. 0.0025 mmol of tetra ethyl ammonium hydroxide, (TENOH, $N(CH_2CH_3)_4OH$, 97 %, 20 wt-%, Aldrich), was added slowly while stirring. In one experiment, 0.00034 mmol

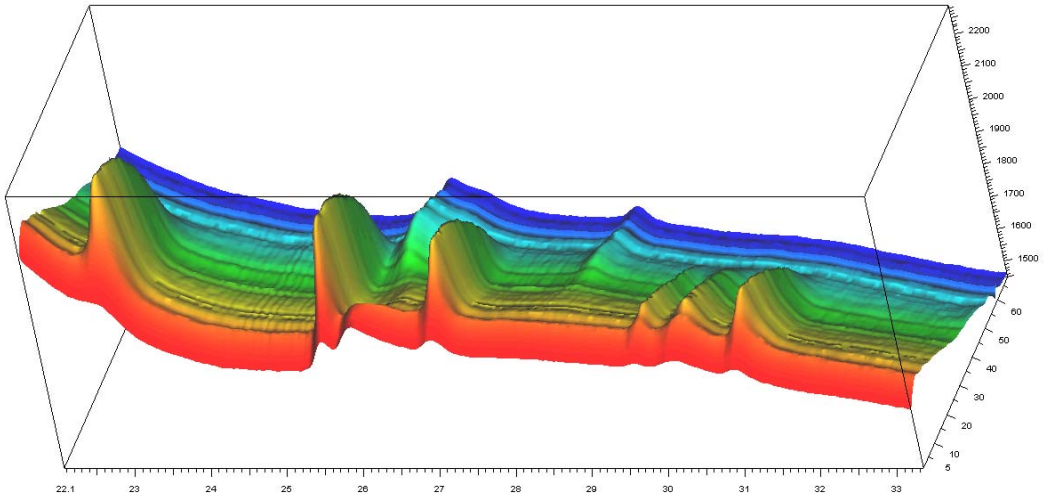

Figure 1. 3-Dimensional representation of in situ powder diffraction data. The x-axis shows the diffraction angle, the z-axis the intensity and the y-axis denotes the different data sets, as they are recorded with increasing temperature.

H_2O_2 (30 wt-%, Norsk Medisindepot) was added to investigate the effect on oxidation of Co^{2+} to Co^{3+} necessary to make the spinel Co_3O_4.

A quartz capillary tube with d=0.7 mm was filled with reactants and mounted on a goniometer head with a Swagelok T-piece. This allows for a N_2 pressure to be applied, and thereby hydrothermal conditions are maintained, when the applied pressure is higher than the vapour pressure of the reaction mixture at the reaction temperature. A pressure of ~10 bar was used. A hot air blower was used to heat a part of the capillary from room temperature to 200 ºC using heating rates of 2, 5 and 10 ºC/minute.

Time-resolved *in situ* experiments (time resolution 107 seconds) were performed using a MAR345 area detector at the Swiss-Norwegian Beam Line BM01A at ESRF.
Figure 1 shows an example of the *in situ* powder diffraction data. The first data set (in front) was collected at room temperature, and the temperature was increased (2ºC/min) to 200ºC. This temperature was held until the amount of products was stabilized.

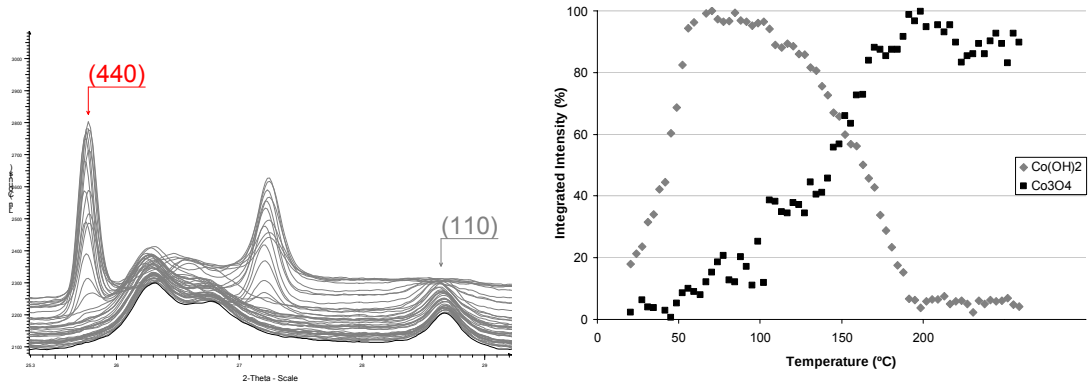

Figure 2. a) The figure shows the (440) peak for Co_3O_4 and the (110) peak for $Co(OH)_2$ in a small area in the sample with a heating rate of 2 °C/min. b) Relative amounts of Co_3O_4 and $Co(OH)_2$ from the integrated intensity of the two peaks.

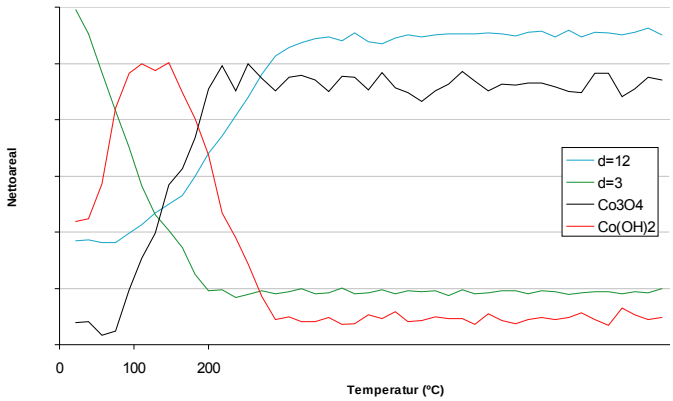

Figure 3. Relative amounts of different phases correlated to Co_3O_4 and $Co(OH)_2$ in the sample with hating rate 10 °C/min.

Some $Co(OH)_2$ is already present at the beginning of the synthesis, and the amount increases with temperature. The formation of Co_3O_4 begins at a higher temperature when the amount of $Co(OH)_2$ almost is at the maximum, see Figure 2. This may indicate that the reaction involves other phases. The existence of additional phases is indicated by the appearance and disappearance of broad features in the powder diffraction patterns. The phases involved could be one or more disordered layered structure. The formation of Co_3O_4 is complete approximately at the same time as a peak at d≈3 Å disappears. The amount of $Co(OH)_2$ reaches zero at the same time as the peak at d≈12 reaches its maximum. The theory of a layered structure can be confirmed by a small peak at d≈1,5 which could very well be the (110)-peak in a hydrotalcite-like phase for example $Co_x^{3+}Co_{1-x}^{2+}(OH)_{2-x}(NO_3)_x \bullet nH_2O$.

The existence of additional phases is indicated by the appearance and disappearance of broad features in the powder diffraction patterns. The phases involved could be one or more disordered layered structure. The formation of Co_3O_4 is complete approximately at the same time as a peak at d≈3 Å disappears. The amount of $Co(OH)_2$ reaches zero at the same time as the peak at d≈12 reaches its maximum. The theory of a layered structure can be confirmed by a small peak at d≈1,5 which could very well be the (110)-peak in a hydrotalcite-like phase for example $Co_x^{3+}Co_{1-x}^{2+}(OH)_{2-x}(NO_3)_x \bullet nH_2O$. However, further studies are necessary to address this.

[1] Nielsen, H.Ø, Master Thesis, Department of Chemistry, Faculty of Mathematics and Natural Sciences, University of Oslo, Norway, **2006**.
[2]Heidi Østbye Nielsen, Ola Nilsen, Helmer Fjellvåg and Poul Norby "Synthesis of Co_3O_4 nanocubes; an *in situ* synchrotron powder diffraction study" In preparation.
[3] Yang, J.; Quaresma, S.; Mei, S.; Ferreira, J. M. F.; Norby, P.; *Key Eng. Mater.* **2005**, *280-283*, 713-716.
[4] Xu, R.; Zeng, H. C.; *Langmuir* **2004**, *20*, 9780-9790.

Figure 4. Schematic drawing of the tetragonal crystal structure of β-MnO_2 viewed along [001].

In situ studies of hydrothermal synthesis of β-MnO_2 nanorods[5] and thermal transformation of cryptomelane nanofibers[6,7].

Hydrothermal synthesis of β-MnO_2 nanorods was followed by means of in situ synchrotron X-ray diffraction of a redox reactions in a mixed $(NH_4)_2S_2O_8$ and $MnSO_4$ solution. The diffraction data, combined with SEM and Raman studies, show that γ-MnO_2 is formed first during the hydrothermal synthesis and subsequently transforms into β-MnO_2 with increasing temperature. The growth of the γ-MnO_2 crystallites follows a nucleation-dissolution-anisotropic growth mechanism. The Raman spectrum of the as-synthesized β-MnO_2 nanorods feature four bands at 759 (B_{2g}), 664 (A_{1g}), 576 (Ramsdellite impurity), and 537 (E_g) cm^{-1}, in agreement with Mn-O lattice vibrations expected for a rutile-type MnO_6 octahedral matrix.

The *in situ* hydrothermal synthesis was performed using a micro-reaction cell. Equal volumes of $(NH_4)_2S_2O_8$ (0.1 M) and $MnSO_4$ (0.1 M) aqueous solutions were mixed under stirring at room temperature. A small amount of the obtained transparent solution was injected into a quartz glass capillary (diameter 0.7 mm) which was mounted in a Swagelok fitting. An internal pressure (N_2) was used in order to maintain hydrothermal

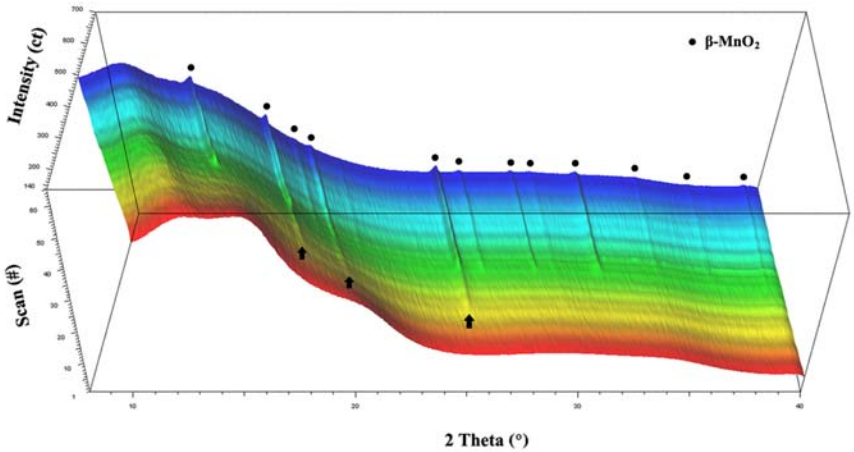

Fig. 5 In situ synchrotron XRD patterns during hydrothermal synthesis of β-MnO_2 nanorods. Reflections from the β-MnO_2 phase are marked with dots. The presence of an intermediate phase is illustrated by arrows. The broad bump between 10 and 20° in 2θ is due to scattering from the quartz glass capillary and solvent.

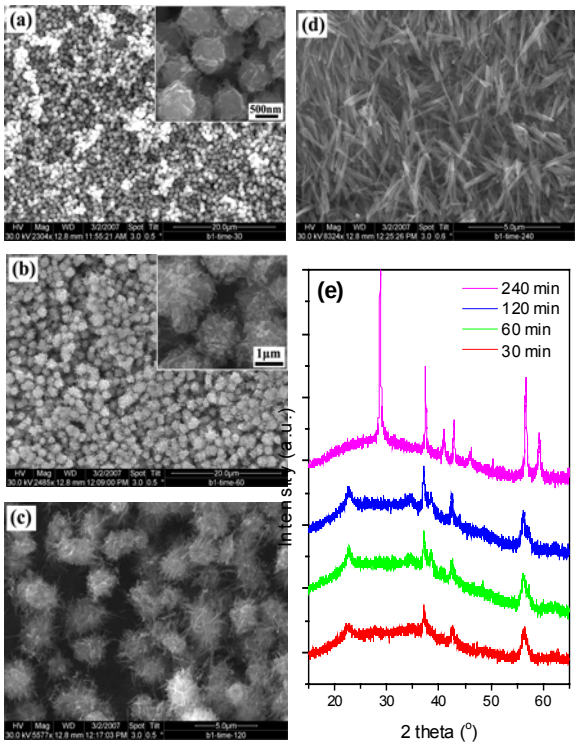

Figure 6. SEM images (a-d) and corresponding XRD patterns (e) of MnO_2 materials prepared by hydrothermal treatment of a mixed solution of $(NH_4)_2S_2O_8$ and $MnSO_4$ at 140°C for 30 min (a), 60 min (b), 120 min (c), and 240 min (d). Insets to (a) and (b) show enlarged pictures. The X-ray wavelength is 0.15406 nm. The XRD patterns are shifted vertically for clarity.

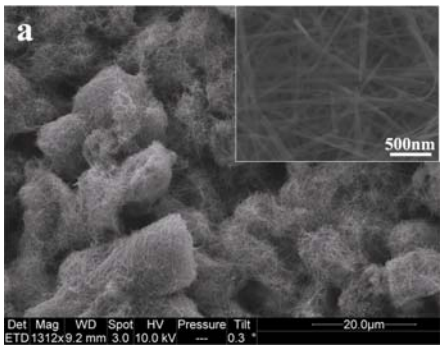

Figure 7. SEM images of cryptomelane nanofibers[6].

conditions and the reaction cell was heated up to 160°C at a rate of 2°C/min.

In situ synchrotron X-ray powder diffraction data were collected at the Swiss-Norwegian Beam Line BM01A, at ESRF ($1 \leq 2\theta \leq 40°$, □ = 0.071096 nm) using a MAR345 detector.

Figure 5 shows a 3-dimensional representation of the time-resolved synchrotron XRD patterns collected during hydrothermal synthesis. Upon gradual increase of the reaction temperature to about 90°C (after 25 scans), an intermediate phase was

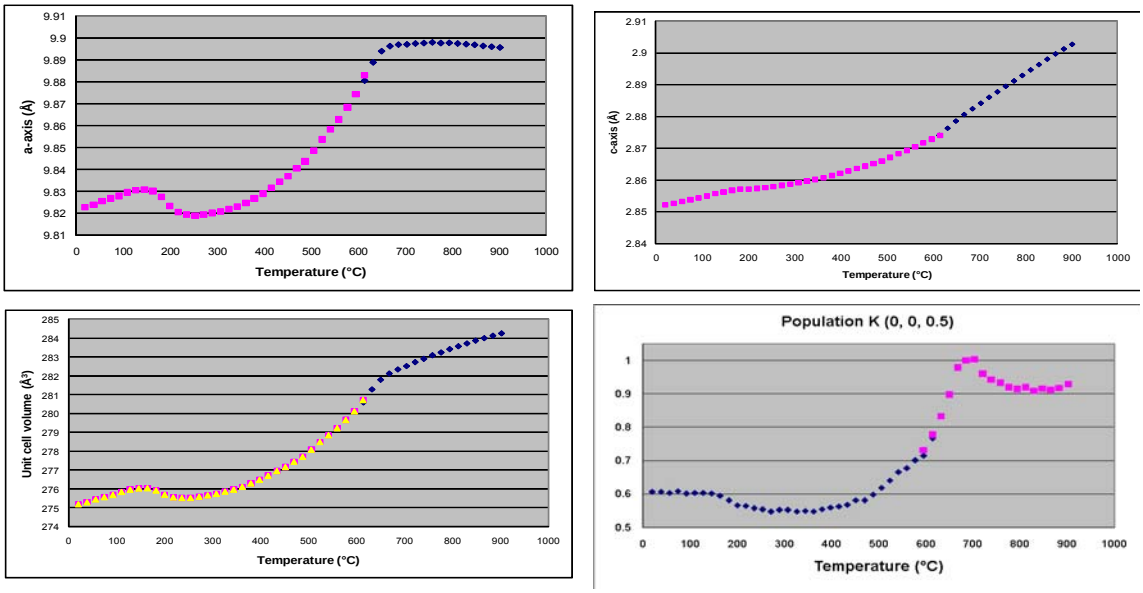

Figure 8. Development in unit cell parameters and potassium content in cryptomelane nanofibers during heating from room temperature to 900C in air.

observed which could be identified as γ-MnO_2. As the reaction temperature increases further to 135°C (after 38 scans), tetragonal β-MnO_2 starts to form.

The reactions were followed also *ex situ* using conventional hydrothermal synthesis. Figure 6 shows SEM images and powder diffraction patterns of the final and intermediate phases.

Other manganese oxide nanomaterials were produced, e.g. cryptomelane nanofibers, K_xMnO_2. This material was prepared by hydrothermal from aqueous solutions of $MnSO_4$ (0.1 M) and $KMnO_4$ (0.1 M). The suspension was heated in a teflon-lined stainless steel autoclave at 140°C for 24 h without shaking or stirring[6].

The thermal transformation of cryptomelane nanofibers was followed by heating in a controlled atmosphere (air or N_2 flow) from 20 to 900°C. Powder diffraction patterns were collected using the MAR345 imaging plate detector. Upon heating, a disproportionation reaction takes place resulting in formation of a potassium rich cryptomelane phase together with bixbyite, Mn_2O_3. By Rietveld refinement of the collected powder diffraction data the structure evolution of the two phases was determined. Figure 8 shows the development in the unit cell parameters and the population of the potassium site in cryptomelane as a function of temperature.

[5] Tao Gao, Poul Norby, and Helmer Fjellvåg "*In situ* studies of hydrothermal synthesis of β-MnO_2 nanorods" In preparation.

[6] Tao Gao, Marianne Glerup, Frank Krumeich, Reinhard Nesper, Helmer Fjellvåg, and Poul Norby "Microstructures and Spectroscopic Properties of Cryptomelane-type Manganese Dioxide Nanofibers" *J. Phys. Chem.* ***C*** **2008**, *112,* 13134–13140

[7] Tao Gao, Poul Norby, and Helmer Fjellvåg "*In situ* studies of thermal transformations of cryptomelane nanofibers" To be published

Antiisostructural phases and anomalous thermoelasticity in In-based alloys

V. Dmitriev, D. Chernyshov, and Ya. Filinchuk
Swiss-Norwegian Beam Lines at ESRF, BP220, 38043 Grenoble, France

Anomalous elastic properties of a IIIA group metal indium, and its unusual for metallic elements crystal structure give rise to intense, both experimental and theoretical, studies. Elemental indium has at ambient conditions a body centered tetragonal structure [$(c/a)_{fct}$ >1] with one atom in a primitive unit cell (Z_p=1). A contraction (negative expansion) occurs in In along a four-fold axis and an expansion in a basal plane with increasing temperature. One could have expected that the tetragonal distortion is removed by application of external pressure. However, high-pressure studies of In revealed the stability of the fct structure [1,2]. Moreover, it lowers the symmetry from tetragonal to orthorhombic at about 45 GPa [3]. Alloying In with IIA group metal Cd (x_{Cd}>5 at.%) and IVA group metal Pb (x_{Pb}>30 at.%) allows not only to remove a tetragonal distortion of the crystal lattice and stabilize a face-centered cubic (fcc) structure [4,5], but it switches the sign of distortion and stabilizes another tetragonal structure (bct') with $(c/a)_{fct}$ <1.

The rich and reliable experimental information accumulated for In-based alloys stimulated, in last decade, numerous theoretical works. However, no mechanism was suggested explaining negative thermal expansion, no approach was elaborated allowing to understand atypical behaviour of tetragonal distortion in the compressed metal.

There is an unexplored aspect of the phase transitions occurring in In-based alloys - they are proper ferroelastic transformations. It allows, therefore, by applying rather simple phenomenological formalism, to uncover the generic features of phase stability and crystal lattice transformations. Such approach is symmetry based and, therefore, model free. Its important advantage consists as well in easy incorporation of different external variables, like pressure, concentration or temperature, so that, for instance, the latter is not restricted to T=0 K.

In situ high-temperature and high-pressure data were obtained at the Swiss-Norwegian Beam Lines (BM1A) of the European Synchrotron Radiation Facility (ESRF, Grenoble, France). X-ray diffraction patterns were collected in angle-dispersive geometry using an image plate detector (MAR345).

It is convenient to classify a phase transition as ferroelastic if it involves a change in crystal system, accompanied by a change in strain owing to the difference in unit cell shape. The experimentally measured strain $\varepsilon_1=(c_t/a_t-1)$ carrying parent cubic lattice to tetragonal one is one of two symmetry equivalent strains

$$\varepsilon_1 = \tfrac{1}{\sqrt{6}}(e_1 + e_2 - 2e_3)\,, \quad \varepsilon_2 = \tfrac{1}{\sqrt{2}}(-e_1 + e_2), \tag{1}$$

The symmetrical combinations of the diagonal components e_i (i=1÷3) of the strain tensor can be, therefore, considered as order-parameter (OP) components for a cubic-to-tetragonal proper ferroelastic transformation. The corresponding non-equilibrium thermodynamic potential is a functional of two polynomials invariant by cubic symmetry group of the parent phase:

$$I_1 = \varepsilon_1^2 + \varepsilon_2^2 = \eta^2\,, \qquad I_2 = \varepsilon_1^3 - 3\varepsilon_1\varepsilon_2^2 = \eta^3 Cos3\varphi\,; \tag{2}$$

The corresponding variational free energy (Landau potential) is

$$F(P,T,\varepsilon_1,\varepsilon_2) \equiv \Phi(P,T,\eta,\varphi) = \Phi_0(P,T) + a_1 I_1 + a_2 I_2 + a_{11} I_1^2 + a_{12} I_1 I_2 + a_{111} I_1^3 + a_{22} I_2^2\,. \tag{3}$$

The equations of state $\partial\Phi/\partial\eta=0$, $\partial\Phi/\partial\varphi=0$ result from the minimization of Φ with respect to the variables η and φ (or F to ε_1 and ε_2), and yield four possible equilibrium structures

0. $\eta=0$ $\{\varepsilon_1=\varepsilon_2=0\}$: *Fm3m* (Z_P=1);

I. $\eta\neq0$, $Cos\varphi=1$ $\{\varepsilon_1=\varepsilon, \varepsilon_2=0;\ e_1=e_2>e_3\}$: *I4/mmm* (Z_P=1, c/a<1);

II. $\eta\neq0$, $Cos\varphi=-1$ $\{\varepsilon_1=\varepsilon, \varepsilon_2=0;\ e_1=e_2<e_3\}$: *I4/mmm* (Z_P=1, c/a>1);

III. $(a_2 + a_{12}I_2 + 2a_{22}I_2)=0$

$\{\varepsilon_1\neq0, \varepsilon_2\neq0, \varepsilon_1\neq\varepsilon_2\}$: *Fmmm* (Z_P=1). (4)

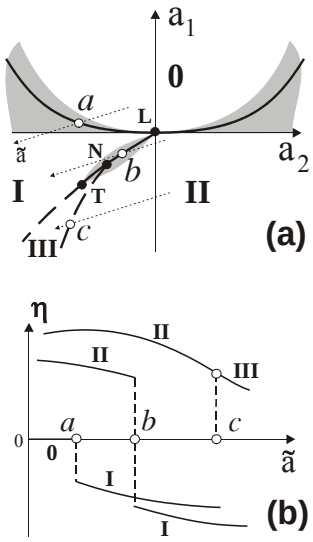

Fig. 1. (a) Phase diagrams corresponding to the thermodynamic potential defined by Eq. (3). Dotted lines denoted a-c are thermodynamic paths, which correspond to different sequences of phases. (b) Order parameter variation for the various paths shown in (a).

The equations of state determine, in addition to the cubic parent phase 0, two low symmetry phases, I and II, with identical tetragonal symmetry. They are associated with opposite values of the equilibrium order parameter components, i.e. phases I and II are *antiisostrural* [6]. The orthorhombic symmetry of phase III is the maximal common subgroup of the symmetry groups of phases I and II.

The space groups of the I and II phases are the same but the sign of the order-parameter components changes from one phase to another [Fig. 1(b)]. In terms of the spontaneous strain tensor components one has on one phase $e_3>e_2=e_1$, whereas in the other phase $e_3<e_2=e_1$ [see Eqs. (4)]. Accordingly, in the case of cubic-to-tetragonal transformation two antiisostructural phases are associated with the opposite signs of the tetragonal distortion (c/a-1). Figure 1(b) shows the shape of $\eta(\tilde{a})$ along thermodynamic paths defined by straight lines $\tilde{a}=\alpha_0 a_1+\beta_0 a_2$ in the (a_1,a_2) plane, which correspond to various sequences of the phases indicated in Fig. 1(a).

The overall phenomenological Landau approach can be tested against available structure data determined at room temperature as a function of pressure, across the In-Pb alloys. The pure indium metal crystallizes in a body-centered tetragonal structure (*I4/mmm*, Z_P=1) [5], which corresponds to a slightly distorted face-centered cubic (fcc) structure with $(c/a)_{fct}$=1.076 [phase II in (6)]. High-pressure x-ray diffraction experiments revealed that the c/a ratio increases with pressure, reaching a maximum around 24 GPa, and then uncommonly decreases with further compression [1]. At 45 GPa Indium transforms to a face-centered orthorhombic (fco) phase *Fmmm* (Z_P=1), which is obtained by a simple orthorhombic distortion of the low-pressure tetragonal phase [3]. One notices that this sequence corresponds to the path *c* in Fig. 1(a). The $In_{.90}Pb_{.10}$ alloy, at ambient conditions, has the same In-type fct structure with c/a>1 (phase II). Under pressure, it undergoes a phase transition to another tetragonal structure, with a discontinuous jump of the axial ratio from c/a>1 (phase II) to c/a<1 (phase I) [7], i.e. it follows the path *b* in Fig. 1(a).

The Pb-enriched alloys $In_{.85}Pb_{.15}$ and $In_{.78}Pb_{.22}$ crystallize in the latter fct' structure (phase I) and show no phase transition up to, at least, 40 GPa [8]. Alloys $In_{1-x}Pb_x$ with 30>*x*>60 at.% have a cubic structure [parent phase 0 in (4)] and, under pressure, transform from fcc (phase 0) to fct' structure with c/a<1 (phase I, path *a*) [9].

Therefore, all above features of the phase evolution in In-Pb alloys are evidently encountered in the framework of the phenomenological model with the Landau potential (3).

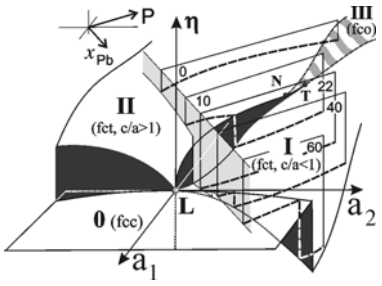

Fig. 2. Equilibrium phase diagram corresponding to the thermodynamic potential (3), in the (a_1,a_2,□) space. Greyish plane is an ambient isobaric plane. Vertical planes are (□,P) isothermal sections corresponding to $In_{1-x}Pb_x$ with different Pb content. Dashed lines in the planes show order parameter □=(c/a-1) as a function of pressure. The numbers indicate the atomic percentage of lead.

Figure 2 shows the phase diagram identical to Fig. 1(a) but complemented with third dimension that is order parameter □. One finds that plane sections of the theoretical diagram [Fig. 1(b) and Fig. 2] perfectly reproduce order parameter, η=(c/a-1), evolution as a function of pressure, experimentally obtained by different authors [1-3,7-8]. The correct mapping of the structural phases and η=(c/a-1) as a function of pressure implies that the symmetry-based theory with nonequilibrium potential (3) gives a unifying picture of phase stability and pressure induced elastic behaviour for $In_{1-x}Pb_x$ alloys. This conclusion encourages us to study pressure- and temperature-induced elastic strains in other In-based alloys, namely $In_{1-x}Sn_x$ and $In_{1-x}Cd_x$, in order to validate the phenomenological model.

An important question, which this study addresses, regards the origin of a remarkable thermoelastic anisotropy in the pure In metal and In-based alloys. Its thermal expansion coefficient α_{11} perpendicular to the tetragonal axis is positive, but the coefficient α_{33} parallel to the axis is negative and decreases with increasing temperature. However, accurate measurements on pure In samples and its alloys with Pb, Sn, and Cd allow us to conclude that above property is characteristic of a tetragonal structure with c/a>1, i.e. of the phase II, but not phase I with c/a<1 (Fig. 3). The sign of □$_{33}$ correlates, therefore, with the sign of ferroelastic OP.

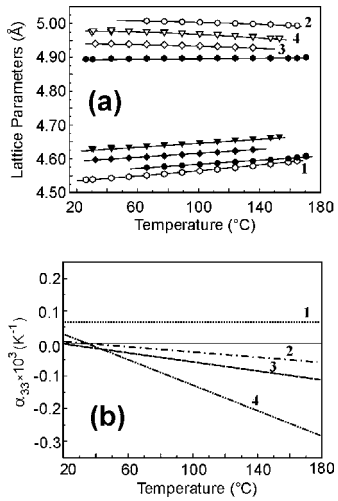

Fig. 3. (a) Thermal expansion of In-based alloys. Circles correspond to $In_{.92}Sn_{.08}$, triangles $In_{.90}Pb_{.10}$, diamonds In, hexagons $In_{.78}Pb_{.22}$. Open spots correspond to the lattice parameter c, closed a. (b) Temperature variation of the principal expansion coefficient □$_{33}$ for $In_{.78}Pb_{.22}$ (1), $In_{.92}Sn_{.08}$ (2), In (3), and $In_{.90}Pb_{.10}$ (4)

Simultaneous heating fct/fct' two-phase mixture in identical conditions provides us with an unambiguous evidence that pressure and concentration play only secondary role in the effect. We have managed to manufacture such a mixture for one of In-Pb alloys at ambient conditions. Following Fig. 2, an alloy with near critical concentration x_{Pb}=10 at.%, at ambient conditions is very close to the fct-fct' transition line, so that the difference in energy between stable II and metastable I should be very small and the corresponding energy barrier should be very tiny. We found that phase content of $In_{.90}Pb_{.10}$ samples depends on the preparation procedure. Original alloy lumps are single-phase, only phase II is present. Although a small

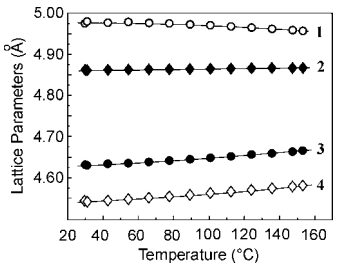

Fig. 4. Temperature variation of the lattice parameters of $In_{.90}Pb_{.10}$ in phases I and II, at ambient pressure: 1 - c_{II}, 2 - a_I, 3 - c_I, 4 - a_{II}.

chip cut with a blade remains single-phase, rasping the lump transforms a part of the sample powder to phase I. Shear stresses, induced by rasping off, promote, therefore, a transition between fct and fct' structures even at ambient conditions. The fct' (I) structure is retained in the sample up to T=135°C (melting point for the alloy is T=150°C), and then irreversibly transforms to fct (II).

Heated now in identical conditions, fct (phase II) and fct' (phase I) structures exhibit, nevertheless, different thermoelastic behaviour. In the stable fct structure a contraction occurs along a four-fold axis, with increasing temperature, while the metastable fct' one shows dilatation in the same direction (Fig. 4).

A total strain induced in a distorted structure by temperature variation consists of two parts: $\varepsilon_T=\varepsilon_{th}+\varepsilon_{OP}$, where ε_{th} corresponds to an ordinary thermal expansion (non-symmetry breaking), and ε_{OP} is a spontaneous strain induced by a ferroelastic phase transition (symmetry breaking). Thermal expansion of a tetragonal structure is entirely characterised by two principal linear expansion coefficients $\alpha_1=\alpha_{11}=\alpha_{22}=(\partial\varepsilon_1/\partial T)=(\partial a/\partial T)/a$, and $\alpha_3=\alpha_{33}=(\partial\varepsilon_3/\partial T)=(\partial c/\partial T)/c$. If a tetragonal structure can be considered as a distorted cubic one, and this is the case for the In alloys, the latter coefficient takes the form $\alpha_3^t=\alpha_1^c+\alpha_{cr}$, where α_1^c is the corresponding coefficient for the cubic structure, and $\alpha_{cr}=\frac{1}{c}\frac{\partial(\Delta c)}{\partial T}\cong\frac{\partial\eta}{\partial T}$ is a "critical" (symmetry breaking) contribution of an order parameter reduced symmetry from cubic to tetragonal. Order parameter values for phases I and II should be found as solutions of the equations of state. Our analysis of experimental data on the In-based alloys concludes that the consideration can be restricted, without loosing of generality, to the vicinity of the Landau point (see Figs. 1 and 2) where fourth-degree terms dominate over six-degree one. It allows, in turn, to restrict the Landau expansion (3) to the forth degree terms. A simplified quadratic equation yields two solutions:

$$\eta_{I,II}=\frac{\mp 3a_2\pm(9a_2^2+32a_1a_{11})^{1/2}}{8a_{11}}, \qquad (5)$$

one corresponding to phase I (upper signs in the numerator), the other to phase II (lower signs).

Remember, that the other our conclusion fixed up the direction of the T-axis parallel to a_1 making all other phenomenological coefficients temperature-independent. Thus, it yields

$$\alpha_{cr}^{I,II}\cong\left(\frac{\partial\eta}{\partial T}\right)_{P,x}=\pm 2\alpha_1\left[9a_2^2+32\alpha_1(T-T_C)a_{11}\right]^{-1/2}. \qquad (6)$$

One finds an additive to the equilibrium cubic expansion coefficient to be positive in phase I (upper sign), but negative in phase II (lower sign). The latter decreases when temperature raises approaching T_C: $\alpha_{cr}\propto(T-T_C)^{-1/2}$. Thus, α_3 may become negative, and it should decrease. Figure 2 clearly shows how the order parameter $\eta=(c_t/a_t-1)$ decreases in phase II with temperature increasing, i.e. lattice parameter c_t decreases approaching

a_t. This negative contribution, becoming dominant, results in the uniaxial contraction (negative expansion) of the tetragonal lattice.

The unified phenomenological theory worked out for In-based alloys maps, therefore, all the structural phases observed experimentally so far, and correctly describes transitions between them. The model discloses the origin of the anomalous elastic anisotropy as being related to the spontaneous strain induced by a proper ferroelastic transition.

Alloying In with IIA and IVA group metals provides an extraordinary example of proper ferroelastic compounds. To the best of our knowledge, this is the first case when variation of external thermodynamical parameters (T, P, *x*) reveals a complete variety of stable phases and phase transitions between them, predicted by a theory with multicomponent order parameter. It is specially applied to direct transitions between antiisostructural phases.

References

[1] K. Takemura, *Phys. Rev. B* **44**, 545 (1991); **[2]** O. Schulte and W. B. Holzapfel, *Phys. Rev. B* **48**, 767 (1993); **[3]** K. Takemura and H. Fujihisa, *Phys. Rev. B* **48**, 8465 (1993); **[4]** *A Handbook of Lattice Spacings and Structures of Metals and Alloys*, ed. W. B. Pearson (Pergamon, Oxford, 1964), vv. 1-2; **[5]** P. Villars and L. D. Calvert, *Pearson's Handbook of Crystallographic Data for Intermetallic Phases* (American Society for Metals, Metals Park, Ohio, 1985); **[6]** P. Toledano and V. Dmitriev, *Reconstructive Phase Transitions in Crystals and Quasicrystals* (World Scientific, Singapore, 1996); **[7]** V. F. Degtyareva et al. *J. Phys.: Condens. Matter* **15**, 1635 (2003); **[8]** V. F. Degtyareva et al. *High Pressure Research* **24**, 551 (2004); **[9]** O. Degtyareva et al. *J. Phys.: Condens. Matter* **13**, 7295 (2001).

Publication

Dmitriev V.P., Chernyshov D., Filinchuk Y.E., Degtyareva V.F. Anti-isostructural phases and anomalous thermoelasticity in In-based alloys: Synchrotron x-ray diffraction experiments and unified phenomenological model. *Phys. Rev. B*, 2007, **75**, 024111.

Structural transformations of light metal borohydrides

Y. Filinchuk, D. Chernyshov, and V. Dmitriev
Swiss-Norwegian Beam Lines at ESRF, BP220, 38043 Grenoble, France

Light metal hydrides are considered as perspective energy carriers for future mobile applications. Hydrogen can be produced from borohydrides of alkaline metals by varing thermodynamic parameters such as temperature and pressure or in the reaction with water. In order to understand the stability and find ways to influence it we studied structure and transformations of $NaBH_4$ and $LiBH_4$ at various temperatures and pressures using single-crystal and powder diffraction techniques.

The ambient pressure fcc α-phase of $NaBH_4$ transforms at ~6 GPa into a closely related tetragonal β-phase, and above 8 GPa into a new orthorhombic γ-phase [1]. We collected synchrotron powder diffraction data for $NaBH_4$ in a diamond-anvil cell up to 11.2 GPa. For a successful structure solution, it was absolutely essential to model the sample texture, including it as a variable in a global optimization. Strong texture indicates an oriented growth of crystallites, specific for the β- to γ-$NaBH_4$ transition. The structure (Figure 1) was solved *ab initio* from diffraction data, using program FOX, with most crystallites having their *a*-axes approximately aligned with the compression direction, and then refined by the Rietveld method. Elimination of the correction for the preferred orientation leads to an increase in R_B from 7.9% to 45%. That means that not only the structure solution, but also the refinement would fail if we did not take the texture into account. Elimination of hydrogen atoms increases R_B from 7.9% to 17%, thus showing that their contribution to X-ray diffraction intensities is sufficient for localization of H-atoms, even from high-pressure synchrotron data.

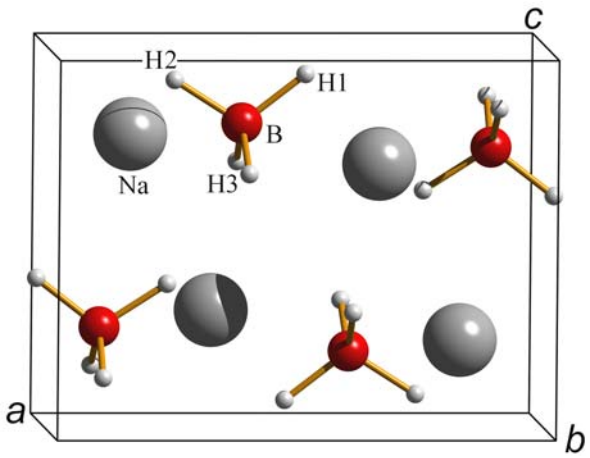

Fig. 1. Crystal structure of γ-$NaBH_4$ at 11.2 GPa, determined ab-initio from diamond-anvil cell synchrotron powder diffraction data.

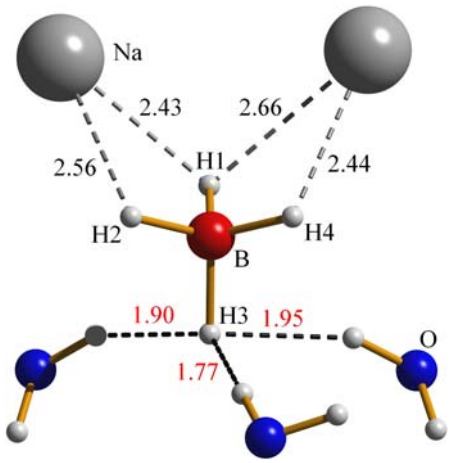

Fig. 2. Dihydrogen bonds in $NaBH_4 \cdot 2H_2O$, determined from synchrotron diffraction on single crystals.

The structure of $NaBH_4 \cdot 2H_2O$ was solved from single crystal diffraction data. It contains sodium cations, which are octahedrally coordinated by four water molecules and two borohydride anions. The BH_4^- anion has a nearly ideal tetrahedral geometry and is bridged with two Na^+ ions via the tetrahedral edges. The structure does

not contain classical hydrogen bonds, but reveals strong dihydrogen O-H$^{\delta+}$…$^{\delta-}$H-B bonds of 1.77-1.95 Å (Figure 2). The H…H distances are much shorter than twice the van der Waals radius of a hydrogen atom (2.4 Å). IR and Raman spectra of $NaBH_4 \cdot 2H_2O$ are consistent with the presence of the dihydrogen bonds for the three O-H groups, and the absence of the dihydrogen bonding for the forth one. An increased accuracy of X-ray diffraction applied to low-Z hydride systems was achieved by introducing a 0.10 Å empirical correction for the B-H distances, which brings H atom positions determined from X-ray diffraction in borohydrides to a direct comparison with those derived from neutron diffraction.

Two $LiBH_4$ polymorphs are known at ambient pressure, with a transition at ~380 K. Substantial theoretical and experimental efforts have been made to characterize their crystal structure. Certain discrepancies remained, however:

- in the low-temperature (LT) phase, all theoretical studies showed nearly ideal tetrahedral geometry of the BH_4 unit, while experiments described it as considerably distorted;
- the high-temperature (HT) phase, reported from synchrotron powder diffraction data to be hexagonal [2], was found unstable by theory; a monoclinic structure has been suggested from *ab initio* calculations [3].

In order to resolve these discrepancies, we studied both $LiBH_4$ phases by synchrotron diffraction on single crystals. We showed that in the LT polymorph the BH_4 group has a geometry of a regular tetrahedron. The space group $P6_3mc$ has been determined unambiguously for the HT phase. Anisotropic displacement ellipsoids, refined also for hydrogen atoms, reveal a libration-like smearing of the BH_4 group, which is well approximated by a TLS model. The revealed disorder suggests that the unaccounted entropy is the reason why *ab initio* calculations have failed to evaluate correctly the stability of the $P6_3mc$ structure.

Synchrotron diffraction of $LiBH_4$ single crystals (Fig. 3) already provides structural results as accurate as those from neutron powder diffraction study of triply (!) isotopically substituted $^7Li^{11}BD_4$ [4]. However, we evaluated even a more accessible technique, synchrotron powder diffraction, for its ability to provide accurate information on the positions of hydrogen atoms. Refinement of the LT structure from the integrated 2D diffraction images (MAR345 detector) resulted in a non-distorted BH_4 geometry. We concluded that the previous powder diffraction studies done with 1D detectors suffer from a poor powder average. The HT phase remains hexagonal from the polymorphic transition at 381K up to decomposition at ~560K. Refinement of the TLS tensor showed that the libration-like disorder of the BH_4 group is nearly

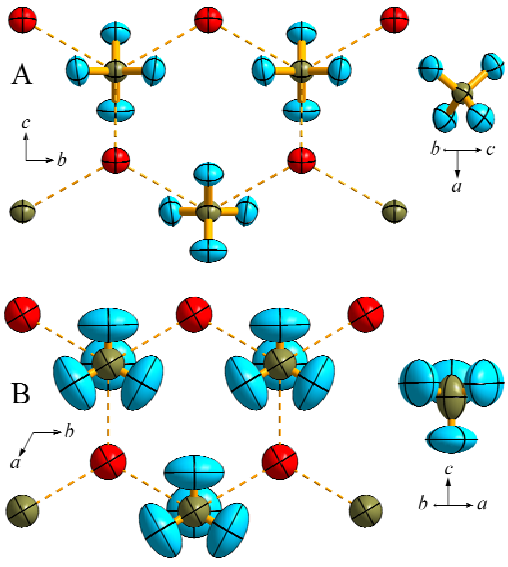

Fig. 3. Six-membered Li-BH_4 rings (left) and BH_4 units (right) in $LiBH_4$ structures. 40% probability ellipsoids are shown. (a) The low-temperature phase at 225 K. (b) The high-temperature phase at 535 K.

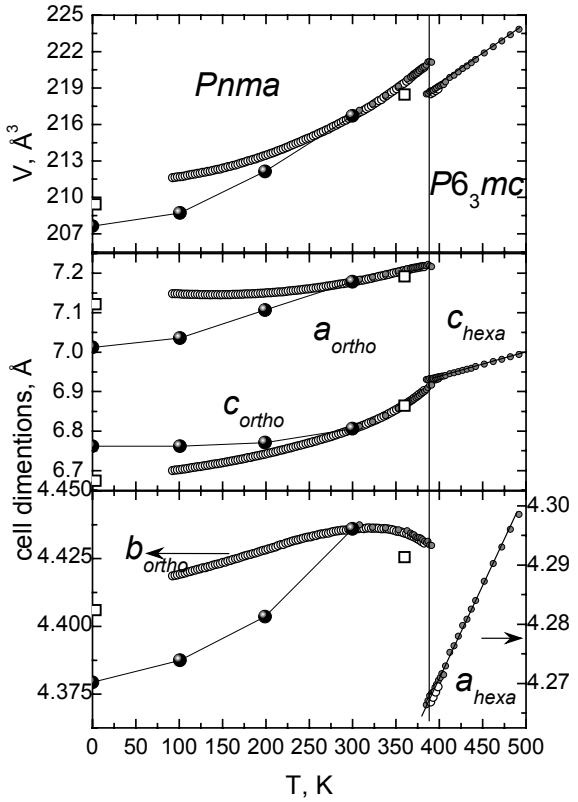

Fig. 4. Unit cell parameters of $LiBH_4$ as a function of temperature. Big dark circles connected by lines represent results of ab-initio calculations [5] scaled to our experimental values at 300 K, open squares represent neutron powder diffraction data [4].

isotropic, in agreement with the single crystal experiment.

In-situ powder diffraction revealed a highly anisotropic thermal expansion of LT $LiBH_4$ (Fig. 4). The cell dimension *b* continuously contracts on heating from 300 K to the transition temperature. The cell parameter *a* deviates from linear dependence below 200 K, shows a minimum at ~150 K and then increases on cooling. Such thermal expansion reflects an anharmonicity of the potential of the crystal binding. A decrease of the unit cell volume upon the LT-to-HT transition phase is remarkable (Figure 4). Thus, the disorder of the borohydride groups and strong lattice anharmonicity were revealed from diffraction data measured at various temperatures. These phenomena, being ignored, lead to a failure of theoretical predictions of structural stability of light borohydrides.

Our studies of $LiBH_4$ in diamond anvil cells showed that its high-pressure phase has a structures different from the one predicted by theory. The structure of a phase observed between 1.2 and 10 GPa has been determined *ab initio* from high-quality powder diffraction data. The new *Ama*2 structure of $LiBH_4$ reveals a novel coordination of the BH_4 anion by Li atoms (Fig. 5, left), and exceptionally short B-H...H-B distaces of 1.9 Å at 2.4 GPa. The DFT-optimized structure indicates the deformation of the BH_4 unit (Figure 5), which is likely to decrease an activation barrier for hydrogen desorption. The internal pressure in the structure may be tuned by a partial chemical substitution. The resulting $LiBH_4$-based substance with *Ama*2 structure may show more favourable hydrogen storage properties than pure $LiBH_4$ and may turn out to be useful for hydrogen storage applications. We suggest the dense

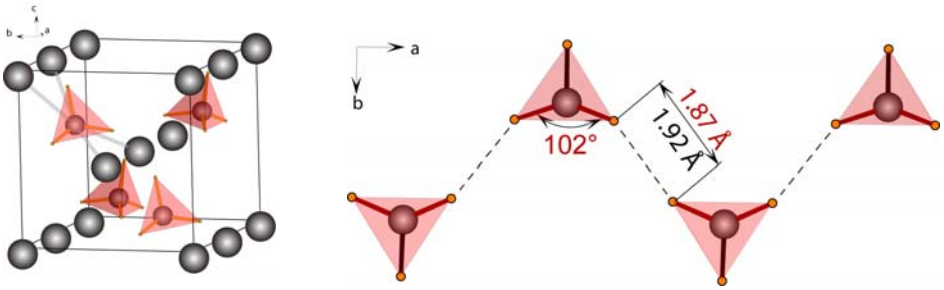

Fig. 5. Square-planar coordination coordination of the BH_4 anion in high-pressure phase of $LiBH_4$ (left). Short H…H contacts (experiment at 2.4 GPa: 1.92 Å; DFT: 1.87 Å) linking the BH_4 groups into chains (above).

structure found in our high-pressure experiments to be targeted for obtaining improved hydrogen storage materials. We have also found a second phase transition into the previously predicted cubic phase of $LiBH_4$, which occurs at higher pressures, above the reach of all previous experiments.

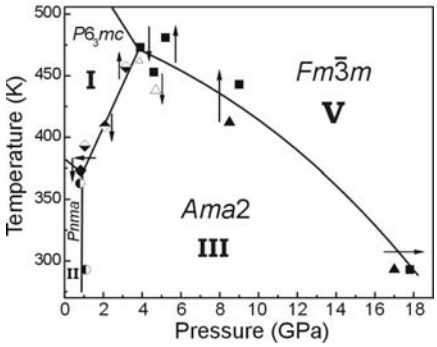

Fig. 6. P-T diagram of $LiBH_4$ based on the diffraction data.

An *in situ* combined high-temperature high-pressure synchrotron diffraction allowed to map a phase diagram of $LiBH_4$ to 10 GPa and 500K (Fig.6). Mechanisms of phase transitions were analyzed using a phenomenological model. It suggests an existence of cation-anion layers in all four known $LiBH_4$ phases. This conclusion is not trivial from purely geometrical point of view, but it can find a rational crystal-chemical explanation. The relative complexity of $LiBH_4$ structures and of the P-T phase diagram can be linked with the directional interaction of the tetrahedral BH_4 groups with spherical metal atoms. We hypothesize that the directional BH_4...M interaction in metal borohydrides leads to a formation of anion-centered complexes, determining structures of individual phases and mechanisms of their polymorphic transformations.

References

[1] R. S. Kumar, A. L. Cornelius, *Appl. Phys. Lett*. **87**, 261916 (2005). [2] J.-P. Soulié, G. Renaudin, R. Černý, K. Yvon, *J. Alloys Compd*. **346**, 200 (2002). [3] Z. Łodziana, T. Vegge, *Phys. Rev. Lett*. **93**, 145501 (2004). [4] M. R. Hartman, J. J. Rush, T. J. Udovic, R. C. Bowman Jr, S.-J. Hwang, *J. Solid State Chem*. **180**, 1298 (2007). [5] T. J. Frankcombe, G. J. Kroes, *Phys. Rev. B*, **73**, 174302 (2006).

Publications

Filinchuk Y., Talyzin A.V., Chernyshov D., Dmitriev V. High pressure phase of $NaBH_4$: crystal structure from synchrotron powder diffraction data. *Phys. Rev. B*, 2007, **76**, 092104.

Filinchuk Y., Hagemann H. Structure and properties of $NaBH_4 \cdot 2H_2O$ and $NaBH_4$. *Eur. J. Inorg. Chem*., 2008, 3127-3133.

Filinchuk Y., Chernyshov D., Nevidomskyy A., Dmitriev V. High-pressure polymorphism as a step towards destabilization of $LiBH_4$. *Angew. Chem. Int. Ed*., 2008, **47**, 529-532.

Filinchuk Y., Chernyshov D., Cerný R. The lightest borohydride probed by synchrotron X-ray diffraction: experiment calls for a new theoretical revision. *J. Phys. Chem. C*, 2008, **112**, 10579-10584.

Dmitriev V., Filinchuk Y., Chernyshov D., Talyzin A.V., Dzwilevski A., Andersson O., Sundqvist B., Kurnosov A. Pressure-temperature phase diagram of $LiBH_4$: synchrotron XRD experiments and theoretical analysis. *Phys. Rev. B*, 2008, **77**, 174112.

STATUS OF FACILITY

A. General Layout and X-ray Optics

The ESRF delivers a 6mrad wide fan of synchrotron radiation to SNBL from bending magnet BM01. A water-cooled aperture plate at the entrance to the Optics Hutch (26m from the source point) divides this beam into two parts of width 2.5mrad and 1.0mrad, with a gap of 2.5mrad between the two beams. The fan of 2.5mrad width supplies the photons to BM1A, while the 1.0mrad beam provides the synchrotron radiation to BM1B. SNBL has been designed from the onset to allow both lines to operate simultaneously, and with a minimum of interaction between the X-ray optics, vacuum system, shielding and controls for each branch line. There are three leaded hutches in series. The first hutch (Optics) contains the majority of the optical components for both branch lines (Figs.1-2). These include two mirrors and a monochromator for BM1A, two separate monochromators for BM1B, as well as various slits, beam position monitors, station shutters, valves and other vacuum components. Although the X-ray optical configurations of both beamlines are fairly conventional, the space restrictions have been a major technical challenge. The available space between the two fans of synchrotron beam which pass through the Optics Hutch is only about 70mm, yet our goal is to operate the two beamlines independently. The two Experimental Hutches are arranged sequentially down the beamline, with the vacuum pipework for BM1A passing through the BM1B Hutch (and through the data acquisition cabin). Two major instruments are positioned in each of the two Experimental Hutches. In BM1A, there is a heavy duty multi-axis diffractometer followed by a large-area image plate detector. BM1B is equipped with a high resolution powder diffractometer and an EXAFS spectrometer. A detailed description of the instrumentation is given below.

The optical configuration of BM1A is a conventional arrangement of vertically collimating mirror, followed by a double crystal Si(111) monochromator and a vertically focusing mirror. The beamline can be configured to operate without mirrors (in order to access higher X-ray photon energies, for example), although some manual realignment of the beamline components is necessary for the changeover. In normal operation, the Rh-coated mirrors provide vertical focusing and harmonic rejection while a sagittally bent second crystal makes the horizontal focusing. It is also possible to interchange the second crystal bending mechanism with a flat crystal mount, if a highly parallel beam is required. The first crystal of the monochromator is water-cooled, as is the first mirror. The mirrors both have a fixed radius of curvature, and the optimum focal spot is roughly circular with a FWHM of about 300 microns. The excellent mechanical and thermal stability of the X-ray optics (at least up to the present maximum current of 200mA) allows us to operate the beamline without a feedback mechanism. Most experiments are carried out in the spectral range from about 10 keV – 20 keV, although higher energies can be accessed if the mirrors are removed. In line with the recommendations of the last beamline review, and following the requests of our user groups, we aim to extend the spectral range of the beamline while maintaining the focussing option. This goal can be achieved by reducing the grazing angle of incidence of the synchrotron beam onto the mirrors from the present value of 3mrad down to 2.5mrad or possibly lower. Although this will involve some loss of total flux in the focussed beam (because of the reduced fraction of the synchrotron beam intercepted by the mirrors), these losses will be offset by the gain in spectra range delivered to the users. It is our goal to extend

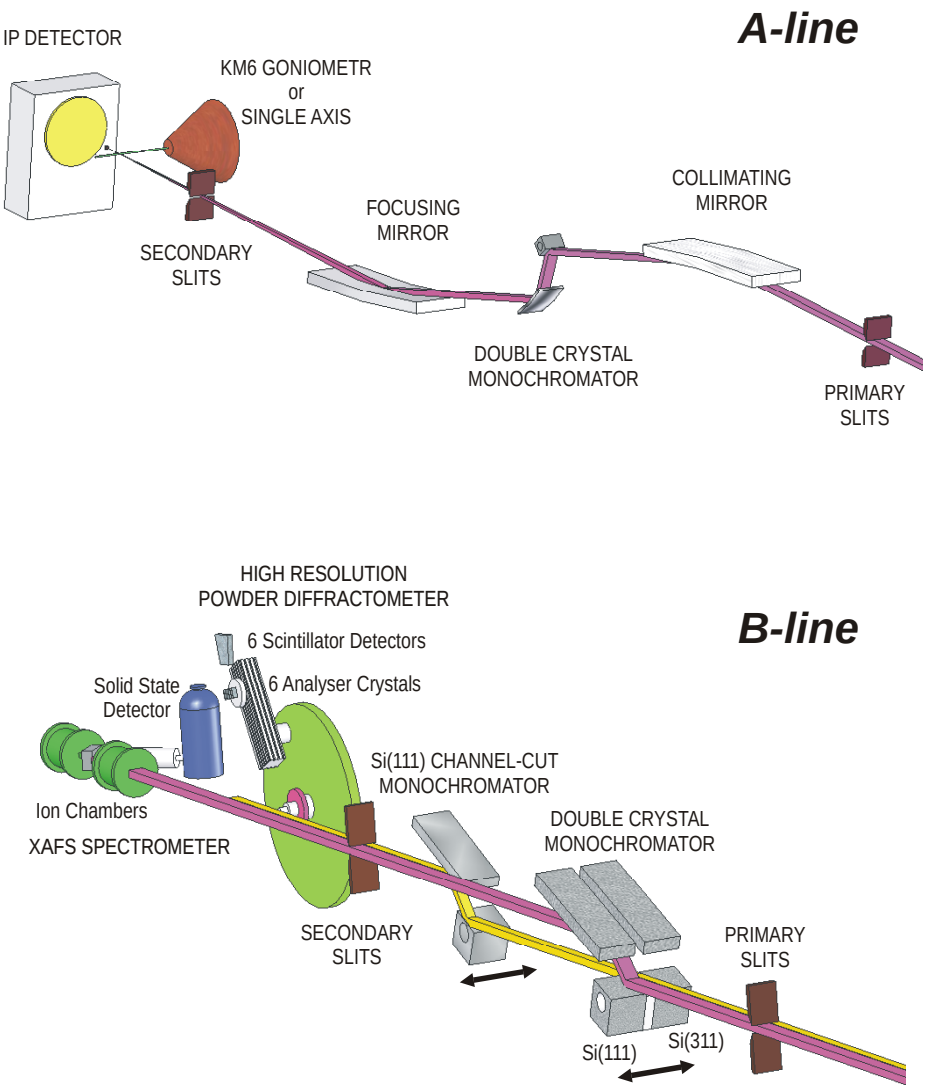

Figure 1. Schematic layout of the SNBL Optics

the spectrum of the focussed beam up to at least 25 keV, and if possible to 30 keV. After several years of operation within the high radiation environment of the monochromator, the motors which drive the sagittal bending mechanism failed due to radiation damage. These DC motors have now been replaced with mechanically more precise (and more reliable) micro-stepping actuators. The more accurate control of the crystal bender has already allowed us to improve the focal quality and hence increase the flux density in the focussed beam.

BM1B is dedicated to High Resolution Powder Diffraction (HRPD) and

Figure 2. General view of the Optics Hutch

EXAFS experiments. A considerable effort has been devoted to the goal of combining these two techniques into quasi-simultaneous measurements. In order to achieve this aim, we have built and integrated two independent, water-cooled monochromators into the optics enclosure (Fig. 3). This allows us to automatically swap between the respective monochromators and hence from HRPD to EXAFS (and vice versa) within a few seconds.

The first monochromator is an unfocused double-crystal monochromator dedicated to EXAFS measurements. It consists of two crystal pairs, Si (111) and Si (311) orientation, mounted on a slide transverse to the incoming beam. By means of this slide, one can quickly choose between the Si(111) and the Si(311) crystal pair, or alternatively select a position that lets the white beam pass by between the two crystals. It is in this configuration that the white beam can reach the following monochromator, which is a Si(111) channel-cut dedicated to High Resolution Powder Diffraction. This channel-cut crystal is again mounted on a transverse slide such that it can be easily moved out of the beam in case that the beam from the first monochromator for EXAFS experiments is required. When

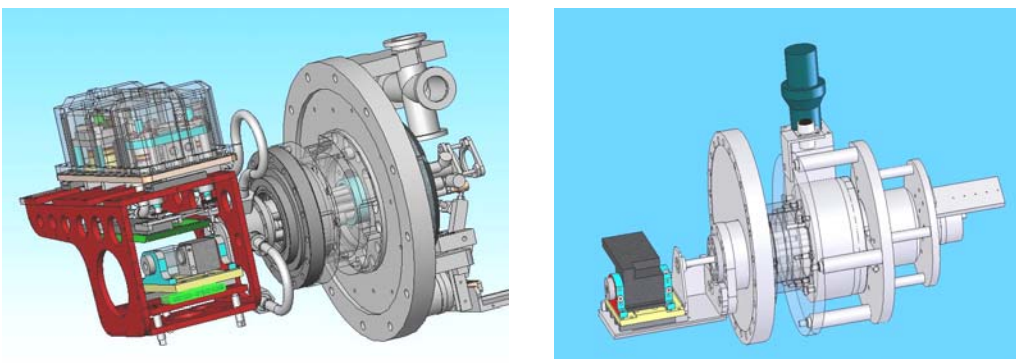

Figure 3 Schematic drawings of the two monochromators on the BM1B branch line

using the EXAFS monochromator, one can quickly choose between the Si(311) high resolution and Si(111) high flux crystal pair. A swap can be performed within a few minutes only (including calibration).

B. Beamline BM1A

After passing through a set of secondary slits within the experimental hutch, the focused synchrotron beam can be delivered to either a multi-axis heavy-duty single crystal diffractometer (KM6 supplied by Oxford Diffraction Ltd) or to the MAR345 Image Plate manufactured by MarResearch GmbH. The MAR345 instrument allows only a single rotation axis for the sample, and a slide provides variable distance between sample and detector. The diameter of the X-ray sensitive plate is 345mm, and a pixel resolution of either 100 or 150 microns can be selected by the user. The KM6 instrument is a κ-diffractometer with the conventional 3 sample rotations (κ, ω and φ) and the detector angle θ. In addition, the diffractometer is mounted on two further rotation tables (ω' and θ') giving an additional degree of freedom to the orientation of both the sample and the detector.

The KM6 multi-axis diffractometer incorporates both a point detector and a large area CCD detector onto the detector arm. The combination of movements available on the KM6 allows us to position the sample in an arbitrary orientation relative to the incoming synchrotron beam (and hence also to its polarization vector), and also to choose freely the angular coordinates of either of the X-ray detectors. This instrument provides a completely generalized platform on which to collect diffraction data. It can be configured either as a vertical or as a horizontal diffractometer, or indeed anywhere in between these scattering planes. Complete surveys of reciprocal space can be rapidly completed using the area detector, while the point detector provides the opportunity to investigate the profiles of individual reflections with high angular resolution. Information concerning the crystal orientation matrix and the diffractometer parameters can be passed smoothly from point detector to area detector configurations. The relatively open architecture of the kappa diffraction geometry is well-suited for the installation of ancillary equipment around the sample. The Figure 4 illustrates an

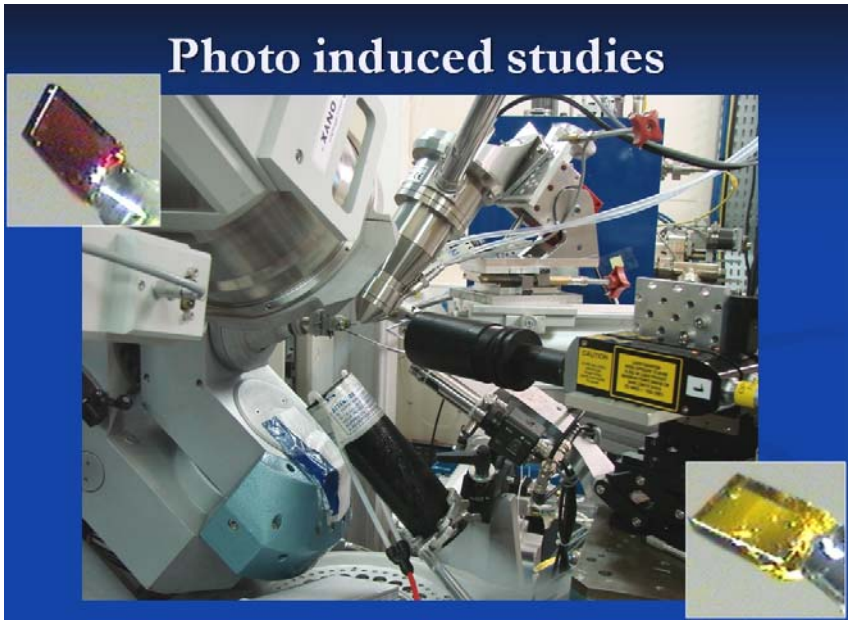

Figure 4. Example of an in-situ experiment carried out on the KM6 diffractometer

in-situ diffraction experiment involving laser excitation of a photo-induced structural phase transition observed at He temperatures.

Apart from a refurbishment of the MAR345 detector, together with some improvements to the optical microscope setup, our image plate system has remained relatively unchanged over the last 5 years. We are now approaching the impressive statistical threshold of 500,000 readout cycles of the image plate. Our efforts have concentrated rather on developing and improving the infrastructure around the sample environment for in-situ experiments. Several types of gas-mixing and gas flow controllers have been used in combination with the image plate detector and the Raman spectrometer. Our upper limit, at present, for gas pressures is around 100 bar (Fig. 5), but we wish to extend this pressure range up to at least 200 bar in the near future (with our ultimate goal of reaching 700 bar H_2 pressure).

Figure 5. Instrumentation for high gas pressure experiments

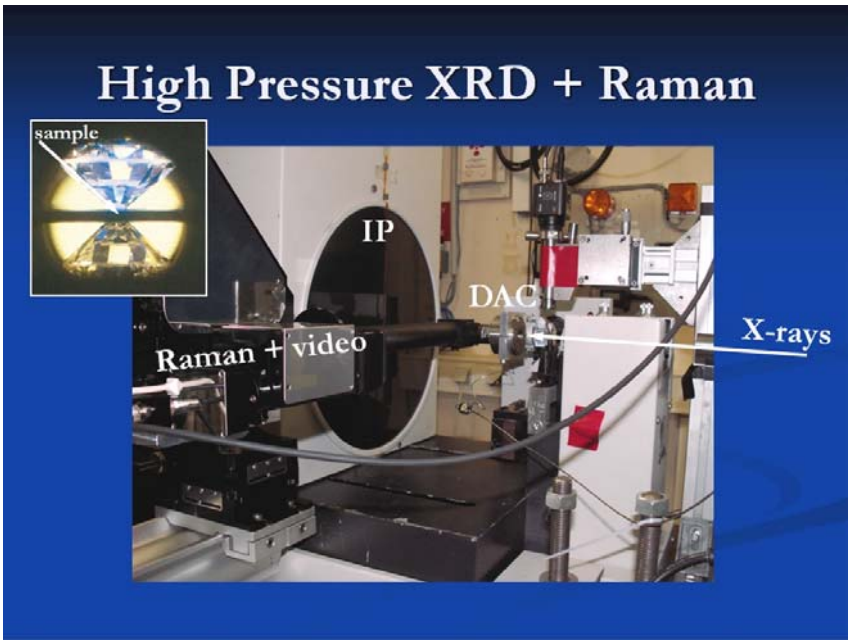

Figure 6.Combined high pressure powder diffraction and Raman experiment on the MAR345

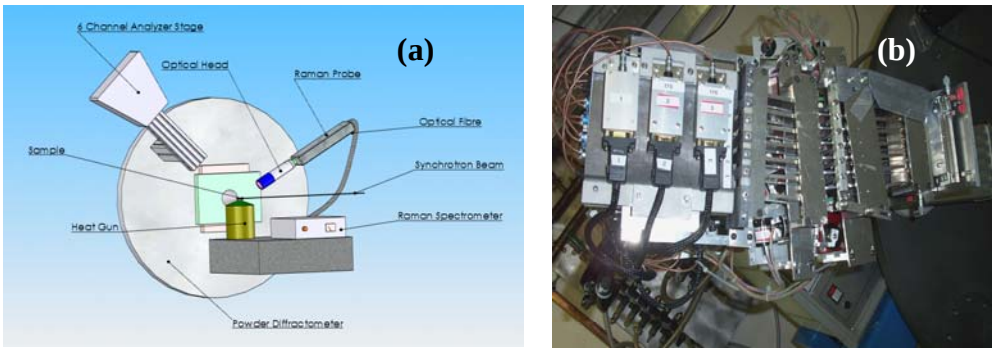

Figure 7. (a) Schematic set-up of the Diffractometer when used in combination with our Raman Spectrometer. (b) Close-up of the analyzer crystal/photomultiplier array. All channels are separated by Soller slits

Amongst the most successful and productive of the techniques which the advantage of the high efficiency and sensitivity of the image plate detector are the high pressure experiments using diamond anvil cells (DACs). These experiments already take up about 10% of the available beamtime on BM1A, and the demand is increasing. A very interesting development concerns the combination of high pressure DAC experiments with the Raman spectrometer, as illustrated in Fig. 6.

C. Beamline BM1B

C.1. The Two Axis High Resolution Powder Diffractometer (HRPD)

The workhorse of the B-station is a two circle powder diffractometer (theta being the outer arm and omega being the inner circle to which the sample is attached. The theta circle is fitted with an array of 6 Si(111) analyzer crystals in front of a second array of 6 scintillation counters (Fig. 7). An analyzer crystal/photomultiplier pair forms one channel. Great care has been taken in order to reduce the angular distance between the channels to a minimum. To do so, the scintillation counters had to be tailor-made (OD 12mm) to allow for a close spacing of 1.1 degrees between two adjacent channels. A second point of consideration was the possibility to reach energies above 30keV. Therefore the scintillator crystals of NaI(Tl) were optimized for efficient photon absorption at high energies. The analyzer set-up consists of a supporting plate holding all six crystals which can be mounted and rotated individually. The supporting plate itself is fixed onto a precision rotary table in order to adjust the Bragg-angle of all analyzer crystals in one rotary motion only. The scintillation counters are assembled to one block, which is mounted onto a second rotary table. Changing the wavelength implies therefore a change of the Bragg-angle of the analyzer array, and a subsequent change of the detectors of twice the Bragg-angle of the analyzer crystals. It takes typically a less than one hour to change from one wavelength to another including a silicon calibration run.

Both circles can be run individually (i.e. in a HRPD run where the sample is spun by an independent sample spinner (omega table stationary) – or in a synchronized way (omega/2theta) which is mainly used for measurements in reflection mode.

C.2. The EXAFS Spectrometer

A) Transmission Measurements

Presently BM1B is equipped with a set of three ion chambers (Hasylab design) for I_0, I_t, I_{ref} respectively. We also possess a small, dedicated gas mixing rack that allows us to change the gas fillings of the ion chambers within a few minutes.

B) Fluorescence Measurements

With additional joint funding from the Swiss and Norwegian partners, we could acquire a 13-element Ge(Li) solid state detector, including the digital acquisition electronics (XIA), in 2003 [Fig. 8(a)]. This detector is frequently used for highly diluted or non-transparent samples.

C.3. Raman

A strong point of SNBL lies in the use of a combination of techniques. This is particularly important for in-situ experiments. In order to understand complex dynamic processes, a maximum of information has to be collected simultaneously. With HRPD being a technique allowing us to measure the long range order and EXAFS being a tool for probing the local structure, vibrational spectroscopy is an ideal non-destructive tool for probing length scales in between these two extremes. Obviously there are additional complementarities to be exploited depending on the system studied. One could cite the different sensitivities of these techniques on surface/bulk or particle size properties. Furthermore, Raman spectroscopy can be applied simultaneously and independently from EXAFS and PD and adds valuable information to a vast number of experiments. The acquisition of a two color (green, red) research grade Raman spectrometer in 2007 made this dream come true. The spectrometer resides in our sample preparation room at the end of the beamline [Fig. 8(b)]. Long optical fibers allow us to link the lasers and the spectrometer to the optical heads in both Experimental Hutches, or, alternatively in the sample preparation room as a stand alone device.

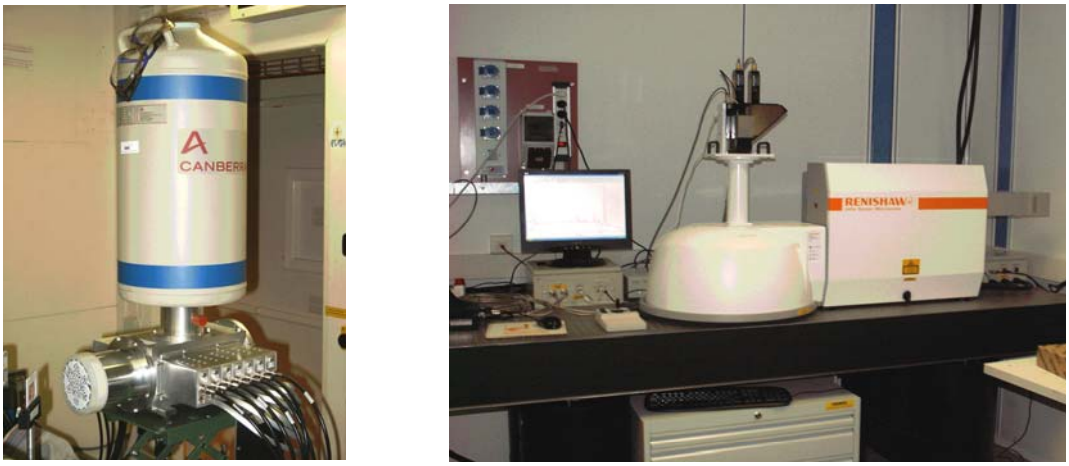

Figure 8. (a) The 13 element solid state detector
(b) The Raman spectrometer as mounted in the sample preparation room

D. Auxiliary equipment available for both beamlines

a. Cryostats

As far as possible we try to adapt our equipment to the need of combining different techniques. As a practical consequence we design our sample environment to be as open and accessible as possible. One example is our He-flow cryostat. By designing the cryostat around our needs, we are in a situation where we can apply all our techniques (Diffraction + EXAFS + Fluorescence + Raman) down to temperatures of 4.5K. An additional, miniature He-flow cryostat has recently been purchased for the KM6 diffractometer, and this cryostat is now being commissioned.

b. Gas mixing and gas flow control

The last year we have also developed together with our user community a gas mixing, flow and measuring system. This system is also fully integrated in the beamline and can distribute gasses to both of our experimental stations. It is a very flexible system capable of adapting to the needs of our wide user community. All gas bottles are stored outside the Experimental Hutches, and a total of 6 different gasses can be supplied via stainless steel pipework to both beamlines. The gas mixing and control system can be completely remote controlled (Figs. 9-10). A mass spectrometer is permanently installed to characterize the gases released after the in-situ reaction. A variety of micro-reaction cells are available for gas pressures up to 100 bar. The majority of the funding for this equipment came from the Catalysis Initiative sponsored by the Norwegian Research Council.

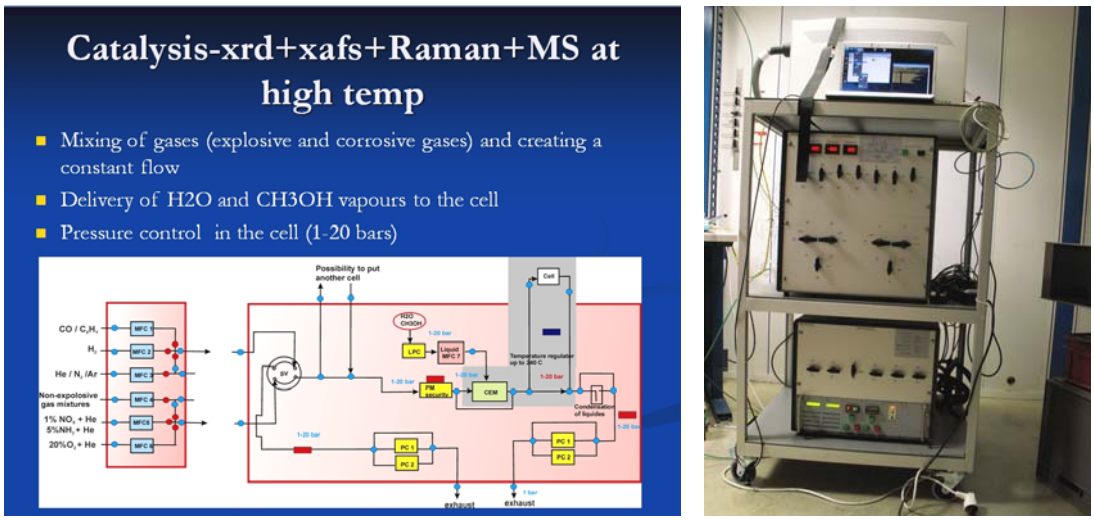

Figure 9. Gas mixing and flow control system (including mass spectrometer)

Figure 10. The array of gas bottles outside the experiment hutches, and the gas mixing system designed for high gas pressures installed on the MAR345 image plate setup

E. Acquisition Software

The increasing complexity of experiments and the flexibility needed to cater for quicker and combined experiments lead us to adopt SPEC as data acquisition software on BM1B in 2004. It also brought the advantage to have direct support from the ESRF software group in order to integrate new instruments and devices. This choice has turned out to be extremely fruitful be it in terms of recently added functionalities (speed, data logging, scanning modes) or in the light of speeding up and synchronizing different measurements or external parameters. As part of the general refurbishment of the beamline, BM1A has now also adopted SPEC for beamline instrument control.

F. SNBL Upgrade and Scientific Perspectives

F.1 Refurbishment and infrastructure

The beamline has recently undergone a major refurbishment of its infrastructure and controls. This refurbishment will be completed in 2008, and it has involved the following items:

- Complete renewal of the vacuum hardware (pumps, gauges, controllers including flow meters for cooling water).

- Replacement of the old vacuum control and interlock system by the latest ESRF standard.

- Complete exchange of the old error prone air-conditioning modules against modern more reliable standard ESRF units.

- Entire rewiring of the mains in order to comply with ESRF standards and French safety regulations.

- Complete replacement of the old UPS power supply (including wiring) against a modern system.

- Replacement of all stepper-motor cards against the new ESRF cards (ICEPAP)

- The latter point induces also a change of the stepper motor control by using the ESRF system (SPEC).

- New floor covering and complete repainting of the radiation enclosures.

In addition to the beamline itself, the experimental equipment has all been checked and serviced (KM6 diffractometer + Onyx CCD and the MAR345 image plate and base). In the case of the computing and motor controls for the experiments, the hardware has been completely replaced. Normal operation of SNBL has been maintained during the entire refurbishment. SNBL is now one of the most up-to-date beamlines at the ESRF concerning all aspects of motor controls and software for instrumentation. One of our major goals is now to automate as many procedures as possible on the beamline (e.g. wavelength change and intensity optimisation, switch between different instrumentation such as powder-to-EXAFS, KM6-to-MAR345 etc.). Despite all of our efforts to maintain the efficiency of the beamline operation, time is inevitably lost when switching between the different instrumentation and functionality of the beamline. In addition, our manpower resources can be heavily committed during such changeover periods. The introduction of more automatic procedures will minimize lost time, reduce the chances of operator error, and release some effort for other tasks.

The SNBL management is following closely the plans for the ESRF Upgrade. Although the CRG bending magnet beamlines are not directly involved in the upgrade, SNBL may well be able to profit from the increased space available when the experimental hall is extended. We have therefore made a preliminary request for additional floor space along the beamline, which would be used to construct an additional laboratory. The need for more space has become particularly pressing since we have now a permanent installation for the Raman spectrometer in our sample preparation laboratory at the end of the beamline. In addition, of course, an increase in the current in the storage ring from the present value of 200mA up to 300mA and beyond would bring a welcome additional flux. Tests with our X-ray optics has demonstrated that we would have no difficultly in taking advantage of the extra photon flux in the incident synchrotron beam.

F.2 Developments and Scientific Perspectives

A. Secondary focussing

Both the KM6/CCD and the MAR345 are routinely used for structure solution from single crystals. Generally, the samples are either too small for lab data collection, or else the crystallography is complex (e.g. incommensurate and modulated structures, twinning, phase transitions). The MAR345 is still used by the Norwegian groups in Oslo and Tromso for data collection on protein crystals. The Oslo group is interested to continue on SNBL with PX measurements because they also use the optical and Raman spectrometers available on BM01. In order to extend further the capabilities for measurements on very small and weakly scattering crystals, we have recently purchased a doubly-curved, graded multi-layer mirror from XENOXS (Grenoble). This mirror can be inserted into the beam close to the sample (Fig. 11), and provides a secondary focus of about 30 microns size (compared to the standard focal spot of about 300 microns). The gain in flux density is about a factor of 30 times. The mirror has a fixed radius, and therefore functions only at photon energies of about 17 keV. This optical configuration will be ideal for working with very small crystals, where the present flux density is too low. It will also be very useful to increase the flux onto samples within a diamond anvil cell, where a beam size of 30 microns will be ideal. A precision multi-axis alignment stage will be required, in order to align the mirror relative to the incoming beam. Test results with this mirror have already shown very promising results, and the plan is to install the mirror on a commercial, muti-axis motorized table in the coming months.

The integrated flux transmitted though the XENOXS mirror will inevitably be reduced by imperfect reflectivity and figure errors, but nevertheless the gain in flux density of a factor of 30 times onto a 30 x 30 μm^2 spot is dramatic (although in practice well within the expected specification). The only drawback of such a

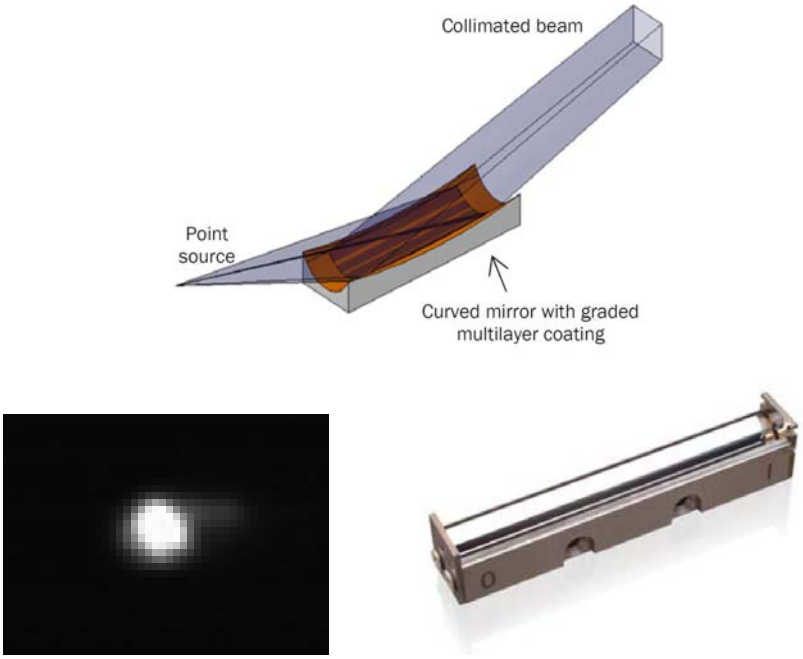

Figure 11. The black rectangle corresponds to the dimensions of the incoming beam arriving on the mirror (about 400 x 600 μm^2), whereas the white spot shows a true image of the focussed beam.

secondary focussing device, apart from the limited operational wavelength range, is an increase in the divergence of the beam arriving on the sample. However, the divergence of the focussed beam increases only to about 1 mrad FWHM, which is quite acceptable for most diffraction experiments. We have found many cases where a sample which was originally planned for measurements on our powder diffraction facility in fact consisted of very small, single crystal grains. Such tiny crystals could until now be measured only with difficulty on SNBL, but the availability of secondary focussing will improve this situation significantly. Similarly, our high pressure experiments using diamond anvil cells, where the typical beam size is about 50 μm, will profit enormously from the increase in flux density on the sample.

B. Powder diffraction with a strip detector

Over the last few years, more and more powder diffraction experiments have been carried out on BM01A, even though this station was originally designed exclusively for single crystal diffraction. In 2007, for example, about 40% of the experiments on BM01A were in fact measurements on powder samples. There are good reasons for the shift in emphasis towards powders:

- When the samples are weakly scattering, or else only very small sample volumes are available, then the combination of focussed beam and highly efficient area detector (MAR345) make some experiments feasible which would otherwise be completely impossible on SNBL. High pressure measurements for samples contained in diamond anvil cells is a good example of this type of experiment. Represents typically about 10% of the total beamtime on BM01A.

- The time resolution of the powder diffraction experiments can be reduced to about 30s using the MAR345 (for some experiments, even shorter times are possible when using a motorized mask placed in front of the image plate). This time resolution matches well the type of experiment in which the temperature is ramped over a wide range (say 120ºC over 2 hours) and a powder pattern collected every 60s. The major drawback of this data collection strategy is the relatively poor angular resolution. Represents typically about 30% of the total beamtime on BM01A.

While the first reason given above will always be valid (unless a complete change in the optical design of BM01B is envisaged), the second reason represents rather a problem with the type of detector system available on the powder diffractometer. Our present arrangement of a set of scintillation detectors positioned behind an array of analyser crystals is intrinsically a relatively slow data collection instrument. The collection times are typically several hours for a full pattern with good statistics. The slow speed of data collection on high resolution diffractometers has long been recognized as a problem at other powder diffraction facilities (e.g. at the SRS, Daresbury, the NSLS Brookhaven and, more recently at Diamond, UK and the Australian Synchrotron) and considerable effort has gone into the development of rapid and efficient X-ray position sensitive detectors. Fortunately, one of the best technical solutions to this problem has emerged from the detector group at the Paul Scherrer Institute in Switzerland. Their electronic strip detector (MYTHEN) has been operating very successfully on the Materials Science beamline at the Swiss Light Source. The narrow width and fine spacing of the individual strips on this detector (50μm pitch with 1280 strips/unit) implies that a dramatic improvement in data collection

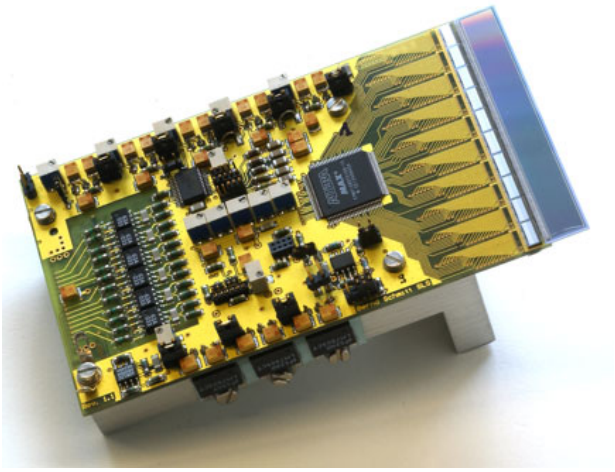

Figure 12. The MYTHEN II detector unit.

speed can be achieved without a significant loss in angular resolution. We are very pleased to acknowledge the generous gift to SNBL from the Paul Scherrer Institute of three of their latest MYTHEN II detector units. Each unit (as illustrated in Fig. 12) covers about 60mm × 8mm, and the three units will be mounted on the SNBL high resolution powder diffractometer. Depending on the distance from the sample, our array of MYTHEN II units can cover either a wide angular range with reduced resolution, or else a more restricted angular range with improved resolution. The time resolution of the powder measurement can be defined by the user in the range between msec to minutes, depending on the goal of the experiment and the required statistics. Completely new types of experiment will become feasible, such as rapid pump-probe, fast switching of electric or magnetic field, polarization switching of liquid crystals and the investigation many other time-resolved physical phenomena which are currently not possible on SNBL.

Silicon sensor:

- 1280 strips
- 8 mm long
- 50 μm pitch
- 300 μm thick.

Read out chip:

- 128 channels
- low noise preamp (noise ≈ 230 e-)
- 18 bit counter
- Read-out time: 250 μs
- Count rate: 1 MHz per channel

SNBL WORKSHOPS

As part of our policy of seeking way to facilitate the exchange of information between the SNBL team and our synchrotron user community, the SNBL management has organized a series of workshops at the ESRF based on themes of current and future interest both to the SN community and a wider scientific audience. The first of these meetings on the topic of nanoscale materials was held in 2006, followed by a workshop on the subject of high gas pressures for *in-situ* experiments in 2007. Both of these meetings were attended by 30-40 participants, including participants from various synchrotron beamlines as well as external users. The recent meeting, which took place in June 2008, continued the theme of *in-situ* experiments, but specifically includes the use of our new Raman spectrometer in combination with x-ray absorption and diffraction measurements. 80 participants, coming from 14 countries, created a very stimulating, constructive and friendly environment for exchanging both scientific and technical know-how and creating new ideas.

- ***In-situ experiments at SNBL using high gas pressures***

A proper understanding of structure-property relationships plays a central role in the design and discovery of novel materials. In many cases, developing the relationship between the structure of a new material and its physical and chemical properties requires that measurements be made under exactly the same *in-situ* conditions of temperature, pressure and atmosphere that match the performance environments of the materials of interest. Examples of research at SNBL leading to a better understanding of materials properties already include catalysis, battery and fuel-cell studies, and solid-state hydrogen storage technology.

The SNBL, in collaboration with our Dutch-Belgian colleagues from DUBBLE, organized a 2-day workshop at the ESRF on 8 and 9 November 2007 on the theme of "High gas pressure experiments". A total of 20 external participants and 10 members of the SNBL and DUBBLE teams attended the Workshop. The external participants came in roughly equal numbers from Norway, Switzerland and the Netherlands, together with some additional invited speakers from the United Kingdom and France.

The main themes of the Workshop included the present status and progress in the field of *in-situ* catalysis experiments, and the current activities in solid-state hydrogen storage research. Both of these subject areas have become the subject of intensive research and development over the last few years, and currently contribute to roughly 50% of the total activities at SNBL. These developments have been driven by the very successful work of the ETHZ groups in Technical Chemistry and the recent Catalysis Initiative led by teams from the Universities of Oslo and Trondheim. In addition, catalysis is supported strongly in the Netherlands (for example in the University of Utrecht and at the Energy Centre of the Netherlands, Petten). Another major area of activity at SNBL concerns energy storage techniques, and in particular solid state hydrogen storage. Several presentations described both the current activities in this field, and the targets for future research. Another research area which was covered during this workshop concerns the use of metal-organic-framework structures

(MOFs), which has recently resulted in several very high profile publications from SNBL.

Interestingly, MOFs can find application both as catalysts and as hydrogen storage materials. In all of these activities, the extension of the current capabilities of SNBL toward experiments under much higher gas pressures is of great topical interest. The various fields of research which require high gas pressures are moving forward rapidly at SNBL. The in-house team has recognized the importance of these techniques, and we have received strong encouragement and financial support from our user community.

- ***SNBL Workshop on simultaneous Raman-X-ray diffraction/absorption studies for the in situ investigation of solid state transformations, and reactions at non ambient conditions.***

X-ray diffraction (XRD) and absorption spectroscopy (XAS) are the principal techniques used to investigate long and short-range order of atoms and molecules in the solid state, respectively. The Raman technique, in contrast, has the ability to probe the length scale between these two extremes. The synergy between these methodologies has attracted application to many scientific studies where the Raman and XRD or XAS techniques have been performed *ex-situ* and independently *in-situ.* The SNBL has further developed their beamline such that these three fundamental probes (XRD-XAS and Raman) can be combined under a wide range of external sample stimuli. This new approach has opened up many new avenues of research and offers vital new detail in the study of materials and solid state sciences. Similar initiatives have recently also been undertaken at other Synchrotrons: APS, SOLEIL, SLS, DIAMOND, BESSY, ANKA, other ESRF beamlines and even in home laboratories. The time was right for a first meeting on combining methods at synchrotrons.

All above mentioned laboratories were represented within the 80 participants as well as industrial partners. The participants, coming to Grenoble June 18-19, 2008, from 14 countries divided over all continents, created a very stimulating, constructive and friendly environment for exchanging both scientific and technical know-how and creating new ideas. Among the speakers were experts in Raman scattering from Biology, Physics and Chemistry. Excellent presentations were for instance given on identification of ligand-bound or intermediate states in Macromolecules, surface versus bulk sensitivity, structure dynamics in combination with computational chemistry, nanostructured ferroelectrics, structure activity relationships on supported oxide catalysts, catalysts in general, micro-focus applications, high throughput screening and possible future developments on sensitivity enhancement. All of the speakers exploited in one form or another the almost endless complementarities between the different techniques dependent on their specific case. The need to combine techniques became with every presentation more and more obvious to anyone in the audience. Many of the presented studies were performed under complex and multiple external stimuli making it impossible to reproduce the experiments on individual machines. It was also extremely stimulating to observe that excellent science has already been performed on the freshly installed installations around the world, consequently indicating a long and bright future for the *in situ, time resolved combination of techniques*.

The SNBL Workshop Proceedings from our 2008 meeting will be published in a special issue of ***Phase Transitions*** (Guest Editors: V.Dmitriev/SNBL and M.Milanesio/Univ. Piemonte Orientale - Italy).

SNBL - FACTS AND FIGURES

BUDGET (in CHF)

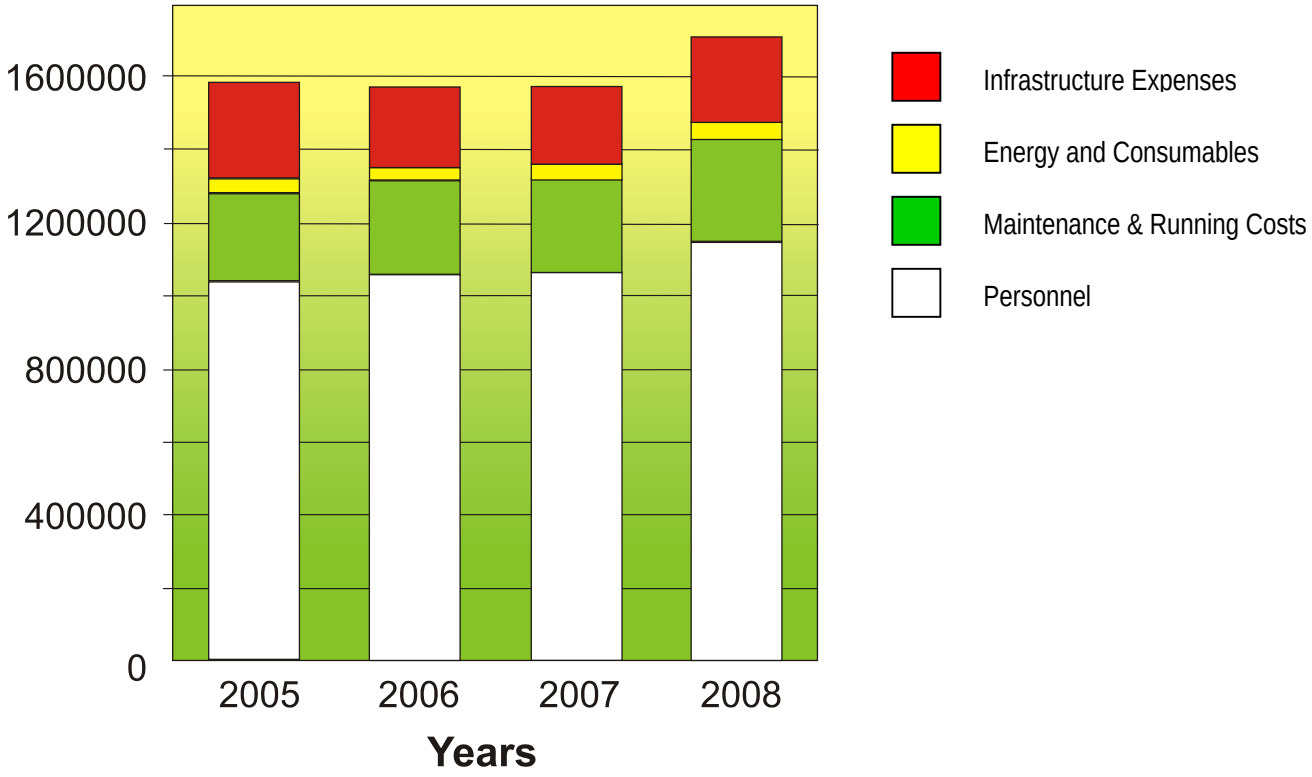

BUDGET in CHF	2005	2006	2007	2008
Personnel	1,037,000.00	1,064,000.00	1,064,000.00	1,144,000.00
Maintenance and Running Costs	240,000.00	257,000.00	257,000.00	275,000.00
Energy and Consumables	35,000.00	38,000.00	45,000.00	50,000.00
Infrastructure Expenses	275,000.00	217,000.00	210,000.00	236,000.00
TOTAL	**1,588,000.00**	**1,576,000.00**	**1,576,000.00**	**1,705,000.00**

INCOME (in CHF)

Income Outside Contract

Income According to Contract

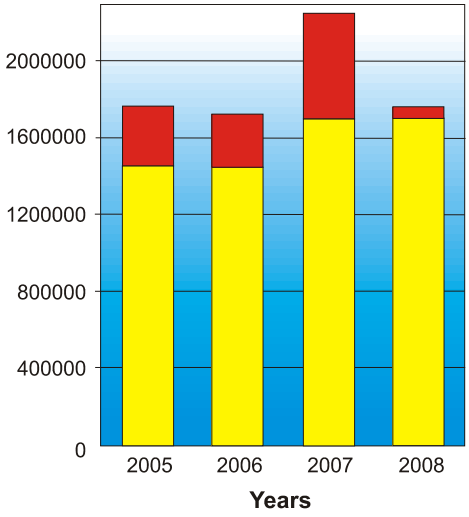

INCOME in CHF	2005	2006	2007	2008
Income According to Contract	1,450,000.00	1,450,000.00	1,698,000.00	1,705,000.00
Income Outside Contract	316,475.00	271,590.00	543,307.00	53,806.00
TOTAL	**1,766,475.00**	**1,721,590.00**	**2,241,307.00**	**1,758,806.00**

EXPENDITURE (in CHF)

Infrastructure Expenses

Energy and Consumables

Maintenance & Running Costs

Personnel

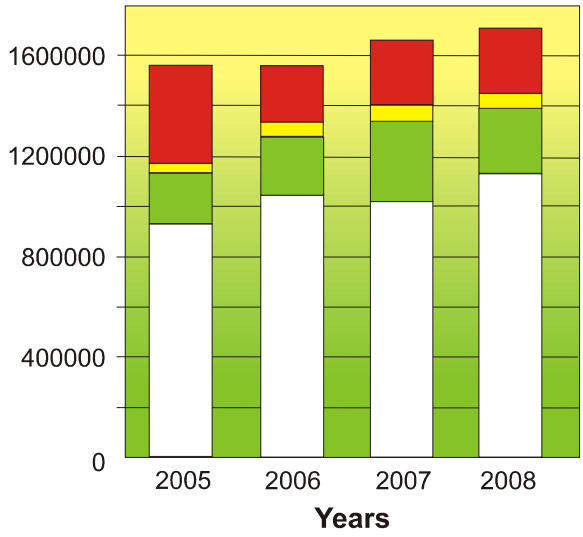

EXPENDITURE in CHF	2005	2006	2007	2008
Personnel	949,000.00	1,056,000.00	1,030,274.00	1,144,000.00
Maintenance and Running Costs	218,000.00	239,000.00	342,000.00	243,157.00
Energy and Consumables	45,000.00	61,000.00	56,000.00	57,246.00
Infrastructure Expenses	269,000.00	219,000.00	240,000.00	247,465.00
TOTAL	**1,481,000.00**	**1,575,000.00**	**1,668,274.00**	**1,691,868.00**

PUBLICATIONS

Publication Rate since start-up of SNBL

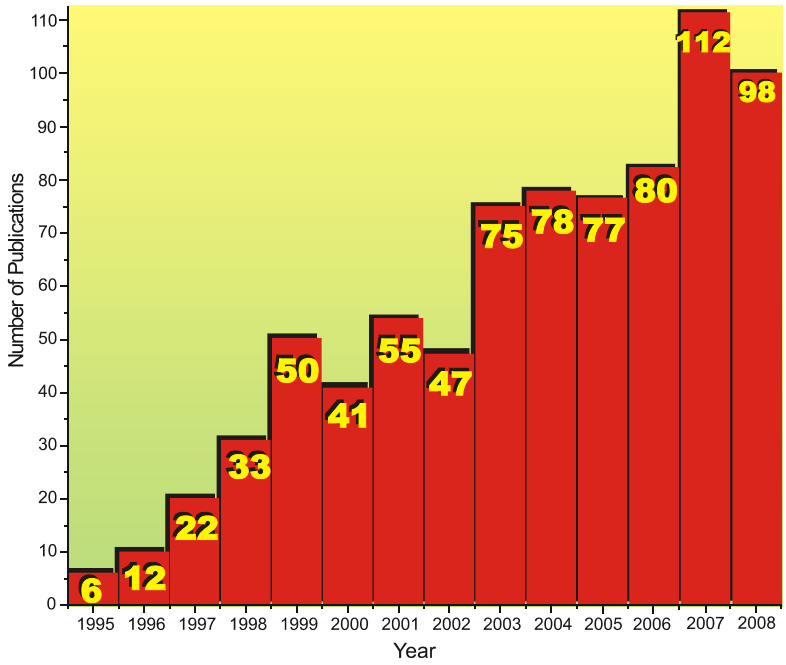

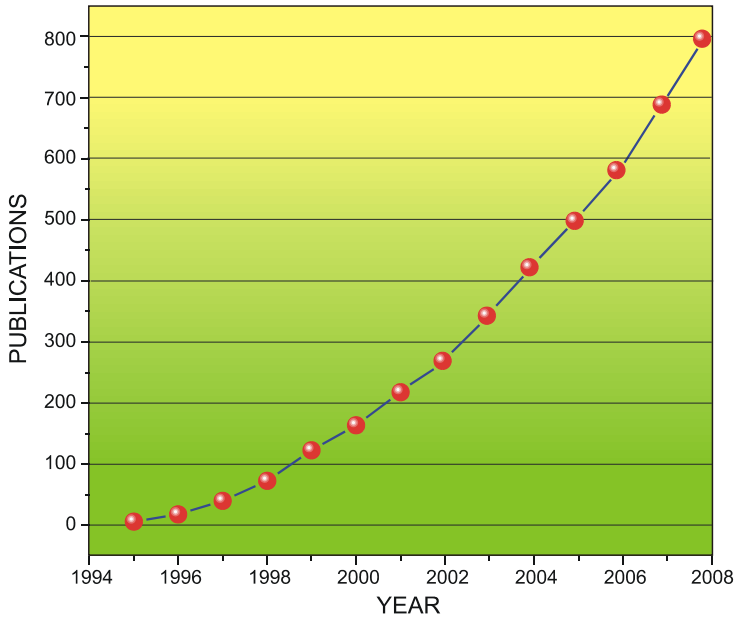

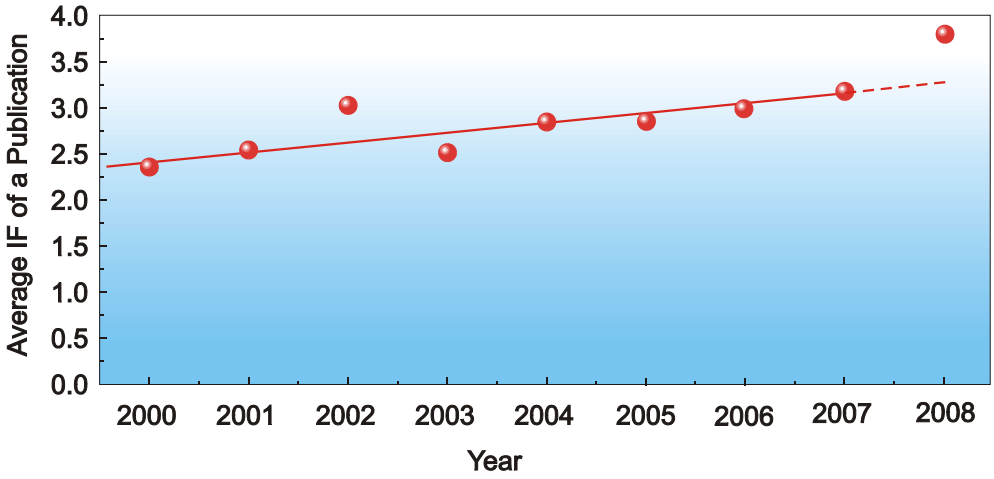

Impact factor of the "average journal" paper produced by the SNBL Users.

List of Publications

2007

2007-1. **Arakcheeva, A., Pattison, Ph., Meisser, N., Chapuis, G., Pekov, I., Thélin, Ph.** *New insight into the pectolite – serandite series: a single crystal diffraction study of Na(Ca$_{1.73}$Mn$_{0.27}$)[HSi$_3$O$_9$] at 293 and 100 K*
Z. Kristallographie, **222**, 12, 696-704, 2007

2007-2. **Arod, F., Pattison, Ph., Schenk, K.J., Chapuis, G.** *Polymorphism in N-Salicylideneaniline Reconsidered*
Crystal Growth & Design, **7**, 9, 1679-1685, 2007

2007-3. **Baerlocher, Ch., Gramm, F., Massüger, L., McCusker, L.B., He, Zh., Hovmöller, S., Zou, X.** *Structure of the polycrystalline zeolite catalyst IM-5 solved by enhanced charge flipping*
Science, **315**, 5815, 1113 - 1116, 2007

2007-4. **Baerlocher, Ch., McCusker, L.B., Palatinus, L.** *Charge flipping combined with histogram matching to solve complex crystal structures from powder diffraction data*
Z. Kristallographie, **222**, 02, 047-053, 2007

2007-5. **Besnard, C., Camus, F., Fleurant, M., Dahlström, A., Wright, J.P., Margiolaki, I., Pattison, P., Schiltz, M.** *Exploiting X-ray induced anisotropic lattice changes to improve intensity extraction in protein powder diffraction: Application to heavy atom detection*
Z. Kristallog., **Suppl.26**, 39-44, 2007

2007-6. **Betti, C. Fois, E., Mazzucato, E., Medici, C., Quartieri, S., Tabacchi, G., Vezzalini, G., Dmitriev, V.** *Gismondine under HP: deformation mechanism and re-organization of the extra-framework species*
Microp. & Mesop. Mater., **103**, 1-3, 190-209 , 2007

2007-7. **Beukes, J. A. , Mo, F., Van Beek, W.** *X-ray induced radiation damage in taurine - A combined X-ray diffraction and Raman study*
J. Phys. Chem. Chem. Phys., **9**, 4609-4724, 2007

2007-8. **Borg, Ø., Rønning, M., Storsæter, S., Van Beek, W., Holmen, A.** *Identification of cobalt species during temperature programmed reduction of Fischer-Tropsch catalysts*
Stud. Surf. Sci. Catal., **163**, 255, 2007

2007-9. **Boccaleri, E., Milanesio, M., Carniato, F., Croce, G., Viterbo, D., Van Beek, W., Emerich, H.** *In situ simultaneous Raman/High-Resolution X-ray Powder Diffraction study of transformations occurring in materials at non-ambient conditions*
J .Appl.Cryst., **40**, 684-693, 2007

2007-10. **Boldyreva, E.** *High-Pressure Polymorphs of Molecular Solids: When Are They Formed, and When Are They Not? Some Examples of the Role of Kinetic Control*
Crystal Growth & Design, **7,** 9, 1662 -1668, 2007

2007-11. **Bourrelly, S., Serre, S., Vimont, A., Ramsahye, N.A., Maurin, G., Daturi, M., Filinchuk, Y. et al.** *A multidisciplary approach to understanding sorption induced breathing in the metal organic framework MIL53(Cr)*
Stud. Surf. Sci. Catal., **170**, 1, 1008-1014, 2007

2007-12. **Brinks, H.W., Brown, C., Jensen, C., Graetz, J., Reilly, J., Hauback, B.C.** *The crystal structure of γ-AlD_3*
J. Alloys & Compounds, **441**, 1-2, 364-367, 2007

2007-13. **Brinks, H.W., Langley, W., Jensen, C.M., Graetz, J., Reilly, J.J., Hauback, B.C.** *Synthesis and crystal structure of ß-AlD_3*
J. Alloys & Compounds, **433**, 1-2, 180-183, 2007

2007-14. **Brugger, J., Etschmann, B., Liu, W., Testemale, D., Hazemann, J.L., Emerich, H. , Van Beek, W. , Proux, O.** *An XAS study of the structure and thermodynamics of Cu(I) chloride complexes in brines up to high temperature (400°C, 600 bars)*
Geochimica et Cosmochimica Acta, **71**, 4920-4941, 2007

2007-15. **Bus, E., Prins, R., Van Bokhoven, J.A.** *Time-resolved in situ XAS study of the preparation of supported gold clusters*
Phys. Chem. Chem. Phys., **9**, 3312 - 3320, 2007

2007-16. **Bus, E., Van Bokhoven, J.A.** *Electronic and Geometric Structures of Supported Platinum, Gold, and Platinum-Gold*
Catalysts Phys. Chem. C, **111**, 27, 9761 -9768, 2007

2007-17. **Caignaert, V., Satya Kishore, M., Pralong, V., Raveau, B., Creon, N., Fjellvåg, H.** *From a 3D protonic conductor $VO(H_2PO_4)_2$ to a 2D cationic conductor $Li_4VO(PO_4)_2$ through lithium exchange*
J. Solid State Chem., **180**, 9, 2437-2442, 2007

2007-18. **Cardoso, M.B., Putaux, J.-L., Nishiyama, Y., Helbert, W., Hytch, M., Silveira, N.P., Chanzy, H.** *Single Crystals of V-Amylose Complexed with -Naphthol*
Biomacromolecules, **8**, 4, 1319 -1326, 2007

2007-19. **Casapu, M., Grunwaldt, J.-D., Maciejewski, M., Baiker, A., Eckhoff, S., Göbel, U., Wittrock, M.** *The fate of platinum in $Pt/Ba/CeO_2$ and $Pt/Ba/Al_2O_3$ catalysts during thermal aging*
J. Catalysis, **251**, 1, 28-38, 2007

2007-20. **Cerny, R., Filinchuk, Y., Hagemann, H., Yvon, K.** *Magnesium borohydride: synthesis and crystal structure*
Ang.Chemie Int. Ed.,**46**, 30 , 5765 - 5767, 2007

2007-21. **Chernyshov, D., Kinduhov, N., Törnroos, K.W., Hostettler, M., Vangdal, B., Bürgi, H. B.** *Coupling between spin conversion and solvent disorder in spin crossover solids*
Phys. Rev. B, **76**, 014406-014413, 2007

2007-22. **Chiarello, G.L., Grunwaldt, J.-D., Ferri, D., Krumeich, F., Oliva, C., Forni, L., Baiker, A.** *Flame-synthesized LaCoO3-supported Pd 1. Structure, thermal stability and reducibility*
J. Catalysis, **252**, 2, 127-136 , 2007

2007-23. **Chiarello, G.L., Ferri, D., Grunwaldt, J.-D.,Forni, L., Baiker, A.** *Flame-synthesized $LaCoO_3$-supported Pd 2. Catalytic behavior in the reduction of NO by H_2 under lean conditions*
J.Catalysis, **252**, 2, 137-147, 2007

2007-24. **Courcot, B. , Firley, D., Fraisse, B. , Becker, P., Gillet, J.-M., Pattison, P., Chernyshov, D. et al.** *Crystal and Electronic Structures of Magnesium(II),*

Copper(II), and Mixed Magnesium(II)-Copper(II) Complexes of the Quinoline Half of Styrylquinoline-Type HIV-1 Integrase Inhibitors
J. Phys. Chem. B, **111,** 21, 6042 -6050, 2007

2007-25. **Cowan-Jacob, S. W., Fendrich, G., Floersheimer, A., Furet, P., Liebetanz, J., Rummel, G., Rheinberger, P., Centeleghe, M., D. Fabbro, Manley, P. W.** *Structural biology contributions to the discovery of drugs to treat chronic myelogenous leukaemia*
Acta Cryst. D **63**, 80-93, 2007

2007-26. **Cunha-Silva, L., Mafra, L., Ananias, D., Carlos, L.D., Rocha, J.,Almeida Paz, F.A.** *Photoluminescent Lanthanide-Organic 2D Networks: A Combined Synchrotron Powder X-ray Diffraction and Solid-State NMR Study*
Chem. Mater., **19**, 14, 3527-3538, 2007

2007-27. **Deledda, S., Hauback, B.C., Fjellvåg, H.** *H-sorption behaviour of mechanically activated Mg–Zn powders*
J. Alloys & Compounds, **446-447**, 173-177, 2007

2007-28. **Denys, R.V., Riabov, B., Yartys, V.A., Delaplane, R.G., Sato, M.** *Hydrogen storage properties and structure of $La_{1-x}Mg_x(Ni_{1-y}Mn_y)_3$ intermetallics and their hydrides*
J. Alloys & Compounds, **446-447**, 166-172, 2007

2007-29. **Denys, R.V., Yartys, V.A., Sato, M., Riabov, A.B., Delaplane, R.G.** *Crystal chemistry and thermodynamic properties of anisotropic $Ce_2Ni_7H_{4.7}$ hydride*
J. Solid State Chem., **180**, 9, 2566-2576, 2007

2007-30. **Dmitriev, V., Chernyshov, D., Filinchuk, Y., Degtyareva, V.** *Antiisostructural phases and anomalous thermoelasticity in In-based alloys: Synchrotron x-ray diffraction experiments and unified phenomenological model*
Phys. Rev. B, **75**, 024111-024119, 2007

2007-31. **Dong, J., Liu, L., Li, J., Li, Y., Baerlocher, Ch., McCusker, L.B.** *Synthesis, characterization and crystal structure analysis of an open-framework zirconium phosphate*
Microp.& Mesop. Mater., **104**, 1-3, 185-191, 2007

2007-32. **Dorokhov, A. V., Chernyshov, D. Y., Burlov, A. S., Garnovskii, A. D., Ivanova, I. S. , Pyatova, E. N. , Tsivadze, A. Y., Aslanov, L. A., Chernyshev, V. V.** *Synchrotron powder diffraction in a systematic study of 4'-[2-(tosylamino)benzylideneamino]-2,3-benzo-15-crown-5 complexes*
Acta Cryst., **B63**, 402-410, 2007

2007-33. **Dragan, F., Bratu, I., Borodi, Gh., Toma, M., Hernanz, A., Simon, S., Cristea, Gh., Peschar, R.** *Spectroscopic investigation of ß-cyclodextrin -metoprolol tartrate inclusion complexes*
J. Incl. Phenom. Macrocyclic Chem., **59**, 1-2, 125-130 , 2007

2007-34. **Dubrovinskaia, N., Solozhenko, V., Miyajima, N., Dmitriev, V., Kurakevych, O., Dubrovinsky, L.** *Superhard nanocomposite of dense polymorphs of boron nitride: Noncarbon material has reached diamond hardness*
Appl. Phys. Lett., **90**, 101912-101915, 2007

2007-35. **Dubrovinsky, L., Dubrovinskaia, N., Crichton, W.A., Mikhaylushkin,S.I., et al.** *Noblest of all metals is structurally unstable at high pressure*
Phys. Rev. Lett. **98**, 045503, 2007

2007-36. **Dyrbeck, H., Hammer, N., Rønning, M., Blekkan, E.A.** *Catalytic oxidation of hydrogen over Au/TiO_2 catalysts*
Topics in Catalysis, **45**, 1-4, 21-24, 2007

2007-37. **Feuerbacher M. et al.** *The Samson phase, ß-Mg_2Al_3, revisited*
Z. Kristallographie, **222**, 6, 259-288 , 2007

2007-38. **Filinchuk, Y., Talyzin, A. V., Chernyshov, D., Dmitriev, V.** *High-pressure phase of $NaBH_4$: Crystal structure from synchrotron powder diffraction data*
Phys. Rev. B, **76**, 092104-092107, 2007

2007-39. **Filinchuk, Y.E., Yvon, K.** *Deuterium site occupancies in $Ce_2Ni_7D_{\sim 4}$ and Comparison with $CeNi_3D_{2.8}$*
J. Alloys & Compounds, **446-447**, 3-5, 2007

2007-40. **Filinchuk, Y., Yvon, K., Emerich, H.** *Tetrahedral D atom coordination of Nickel and evidence for anti-isostructural phase transition in orthorhombic $Ce_2Ni_7D_{\sim 4}$*

Inorg. Chem., **46**, 2914-2920, 2007

2007-41. **Frunz, L., Prins, R., Pirngruber, G.D.** *Mimicking the Active Center of Methane-monooxygenase by Metal-Peptide Complexes Immobilized on Mesoporous Silica*
Chem. Mater., **19**, 17, 4357 -4366, 2007

2007-42. **Giannici, F. , Longo, A., Deganello, F., Balerna, A., Arico, A.S., Martorana, A.** *Local environment of Barium, Cerium and Yttrium in $BaCe_{1-x}Y_xO_{3-}$ ceramic protonic conductors*
Solid State Ionics, **178**, 7-10, 587-591, 2007

2007-43. **Gieck, C., Bisio, C., Marchese, L., Filinchuk, Y., Da Silva, C.E., Pastore, H.O.** *Layered Assembly of Organic Molecules and Host-Guest Interactions in a CAL-1 Chabasite-Type Precursor of H-SAPO-34 Catalysts*
Angew. Chem. Int. Ed., **46**, 8895 - 8897, 2007

2007-44. **Grove, H., Sørby, M.H., Brinks, H.W., Hauback, B.C.** *In Situ Synchrotron Powder X-ray Diffraction Studies of the Thermal Decomposition of β- and γ-AlD_3* J. Phys. Chem. C, **111**, 44, 16693 -16699, 2007

2007-45. **Grunwaldt, J.-D., Van Vegten, N., Baiker, A.** *Insight into the structure of supported palladium catalysts during the total oxidation of methane*
Chem. Commun., 4635-4637, 2007

2007-46. **Grzechnik, A., Gesland, J.-Y., Friese, K.** *High-pressure behaviour of Li_2CaHfF_8 scheelite*
J. Phys.: Condens. Matter, **19**, 096215-0962225, 2007

2007-47. **Gu, Q.F., Krauss, G., Grin, Yu., Steurer, W.** *Comparative high-pressure study and chemical bonding analy sis of Rh_3Bi_{14} and isostructural $Rh_3Bi_{12}Br_2$*
J. Solid State Chem., **180**, 933-941, 2007

2007-48. **Haas, S., Batlogg, B., Besnard, C., Schiltz, M., Kloc, C., Siegrist, T.** *Large uniaxial negative thermal expansion in pentacene due to steric hindrance*
Phys. Rev. B **76,** 205203-205208, 2007

2007-49. **Hafizovic, J., Krivokapic, A., Szeto, K.C., Jakobsen, S. et al.** *Tailoring the Dimensionality of Metal–Organic Frameworks Incorporating Pt and Pd. From Molecular Complexes to 3D Networks*
Cryst. Growth Des., **7**, 11, 2302–2304, 2007

2007-50. **Hammer, N., Kvande, I., Chen, D., Rønning, M.** *Au–TiO_2 catalysts stabilised by carbon nanofibres*
Catalysis Today, **122**, 3-4, 365-369, 2007

2007-51. **Hammer, N., Kvande, I., Chen, D., Van Beek, W., Rønning, M.** *Identification of valence shifts in Au during the water-gas shift reaction*
Topics in Catalysis, **45**, 1-4 , 2007

2007-52. **Hammer, N., Kvande, I., Xu, X., Gunnarsson, V., Tøtdal, B., Chen, D., Rønning, M.** *Au–TiO_2 catalysts on carbon nanofibres prepared by deposition-precipitation and from colloid solutions*
Catalysis Today, **123**, 1-4, 245-256 , 2007

2007-53. **Hannemann, S., Casapu, M., Grunwaldt, J.-D., Haider, P., Trüssel, P., Baiker, A. , Welter, E.** *A versatile in situ spectroscopic cell for fluorescence/transmission EXAFS and X-ray diffraction of heterogeneous catalysts in gas and liquid phase*
J. Synchrotron Rad., **14**, 345-354, 2007

2007-54. **Helmholdt, R. B., Sonneveld, Ed J., Vande Velde, Ch. M. L., Blockhuys, F., Lenstra, A. T. H., Geise, H. J., Peschar, R.** *Structures of tetrabromothiophene and tetrabromoselenophene: the influence of the heteroatom on the heterophene packing*
Acta Cryst. B **63**, 5, 783-790

2007-55. **Hensen, E.J.M., Van der Meer, Y., Van Veen, J.A.R., Niemantsverdriet, J.W.** *Insight into the formation of the active phases in supported NiW hydrotreating catalysts*
Appl. Catalysis A: Gen., **322**, 16-32, 2007

2007-56. **Hersleth, H.-P., Uchida, T., Røhr, Å. K.,Teschner, Th., Schünemann, V., Kitagawa, T. et al.** *Crystallographic and spectroscopical studies of peroxide-derived myoglobin compound II - Occurrence of Protonated Fe(IV)O*

J. Biol. Chem., **278**, 23372 – 23386, 2007

2007-57. **Hong, S. B., Min, H.-K., Shin, Ch.-H., Cox, P.A., Warrender, S.J., Wright, P.A.** *Synthesis, Crystal Structure, Characterization, and Catalytic Properties of TNU-9*
J. Am. Chem. Soc., **129**, 35, 10870 -10885, 2007

2007-58. **Janáková, S., Salavcová, L., Renaudin, G., Filinchuk, Y., Boyer, D., Boutinaud, Ph.** *Preparation and structural investigations of sol–gel derived Eu^{3+}-doped $CaAl_2O_4$*
J. Phys. & Chem. of Solids, **68**, 5-6, 1147-1151, 2007

2007-59. **Joubert, J.-M., Cerný, R., Emerich, H.** *Mixed site occupancies in μ-Zr-Nb-Al by resonant powder diffraction*
Z. Kristallog., **Suppl.26**, 311-316, 2007

2007-60. **Kalisz, M., Novak, M.A., Pinheiro, C.B., Florencio, A.S., Chapuis, G., Caneschi, A., Vaz, M.G.F.** *Synthesis, Structural and Magnetic Characterization of a New Copper(II)-Nitronyl Nitroxide Radical Complex*
J. Brazilian Chem. Soc., **18**, 5, 916-923, 2007

2007-61. **Kantor, A., Kantor, I., Kurnosov, A., Kuznetsov, A., Dubrovinskaia, N., Krisch, M., Bossak, A., Dmitriev, V. et. al.** *Sound wave velocities of fcc Fe-Ni alloy at high pressure and temperature by mean of inelastic X-ray scattering*
Phys. Earth & Planetary Inter., **164**, 1-2, 83-89, 2007

2007-62. **Karau, F. W., Seyfarth, L., Oeckler, O., Senker, J., Landskron, K., Schnick, W.** *The Stuffed Framework Structure of SrP_2N_4: Challenges to Synthesis and Crystal Structure Determination*
Chem. - A Eur. J., **13**, 24 , 6841 - 6852, 2007

2007-63. **Karen, P., Gustafsson, K., Lindén, J.** *$EuBaFe_2O_{5+\square}$: Valence mixing and charge ordering are two separate cooperative phenomena*
J. Solid State Chem., **180**, 1, 148-157, 2007

2007-64. **Kimmerle, B., Grunwaldt, J.-D., Baiker, A.** *Gold catalysed selective oxidation of alcohols in supercritical carbon dioxide*
Topics in Catalysis, **44**, 1-2, 285-292, 2007

2007-65. **Knudsen, K.D., Hemmingsen, P.V., Mo, F.** *Temperature-induced structural changes in some random ethylene/1-hexene copolymers*
Polymer , **48**, 11, 3148-3161, 2007

2007-66. **Krauss, G., Gu, Q.F., Katrych, S., Steurer, W.** *In situ study of icosahedral Zn–Mg–Dy and Co-rich decagonal Al–Co–Ni at high pressures and high temperatures*
J. Phys.: Condens. Matter., **19**, 116203-116214, 2007

2007-67. **Krstic, V., Rikken, G.L.J.A., Kaempgen, M., Roth, S., Beukes, J.A.** *Effects of geometry of nano-structured materials on their thermal expansion: tellurium nanocylinders as model sysyem*
Int. J. Materials and Structural Integrity, **1**, 1/2/3, 2007

2007-68. **Krstic, V., Rikken, G.L.J.A., Kaempgen, M., Roth, S., Beukes, J.A.** *Tellurium Nanocylinders under Pressure: Effects of the Geometry of Nanostructures*
Advanced Materials, **19**, 8 , 1101 - 1104, 2007

2007-69. **Kuznetsov, A. Yu. , Dmitriev, V., Volkova, Y., Kurnosov, A., Dubrovinskaia, N., Dubrovinsky, L.** *In-situ combined X-ray diffraction and electrical resistance measurements at high pressures and temperatures in diamond anvil cells*
High Pressure Research, **27**, 2, 213 - 222, 2007

2007-70. **Laufek, F., Pazout, R. , Makovicky, E.** *Crystal structure of owyheeite, $Ag_{1.5}Pb_{4.43}Sb_{6.07}S_{14}$: refinement from powder synchrotron X-ray diffraction*
Eur. J. Mineralogy, **19**, 4, 557-566(10), 2007

2007-71. **Legrand, V., Pillet, S., Weber, H.-P., Souhassou, M. , Létard, J.-F., Guionneau, P., Lecomte, C.** *On the precision and accuracy of structural analysis of light-induced metastable states*
J. Appl. Cryst., **40**, 1076-1088, 2007

2007-72. **Leiros, H.-K. S., Pey, A. L.,Innselset, M., Moe, E., Leiros, I., Steen, I. H., Martinez, A.** *Structure of phenylalanine hydroxylase from Colwellia psychrerythraea 34H; a monomeric cold active enzyme with local flexibility around the active site and high overall stability*

J. Biol. Chem, **282**, 30, 21973-21986, 2007

2007-73. **Maehlen, J.P., Yartys, V.A., Denys, R.V.,Fichtner, M. , Frommen, Ch., Bulychev, B.M., Pattison, P., Emerich, H., Filinchuk, Y.E., Chernyshov, D.** *Thermal decomposition of AlH_3 studied by in situ synchrotron X-ray diffraction and thermal desorption spectroscopy*
J. Alloys & Compounds, **446-447**, 280-289, 2007

2007-74. **Maehlen, J.P., Yartys, V.A., Riabov, A.B., Budziak, A., Figiel, H., Zukrowski, J.** *Synchrotron X-ray diffraction study of $ErMn_2D_2$*
J. Alloys & Compounds, **437**, 1-2, 140-145, 2007

2007-75. **Malcherek, Th.** *A structural phase transition in NaTaOGeO4 and its relation to phase transitions in titanite*
Acta Cryst. B, **63**, 4, 545-550, 2007

2007-76. **Marchal, C., Filinchuk, Y., Imbert, D., Bünzli, J.-C. G., Mazzanti, M.** *Toward the Rational Design of Lanthanide Coordination Polymers: a New Topological Approach*
Inorg. Chem., **46**, 16, 6242 -6244, 2007

2007-77. **Margiolaki, I., Wright, J.P., Fitch, A.N., Fox, G.C. et al.** *Powder diffraction studies on proteins: An overview of data collection approaches*
Z. Kristallog., **Suppl.26**, 1-13, 2007

2007-78. **Martinelli, A., Roberta, M.** *Cimberle Evolution of the structure, microstructure and physical properties of $RuSr_2GdCu_2O_8$ as a function of the thermal treatment*
Z. Kristallogr., **222**, 9, 459-465, 2007

2007-79. **Massüger, L., Baerlocher, Ch., McCusker, L.B., Zwijnenburg, M.A.** *Synthesis and structure analysis of the layer silicate DLM-2*
Microp. & Mesop. Mater., **105**, 1-2, 75-81, 2007

2007-80. **Meisser, N., Schenk, K., Berlepsch, P., Brugger, J., Bonin, M., Criddle, A., Thélin, P., Bussy, F.** *Pizgrischite, $(Cu,Fe)Cu_{14}PbBi_{17}S_{35}$, a new sulfosalt from the Swiss Alps: description, crystal structure and occurrence*
Canadian mineralogist, **45**, 1229-1245, 2007

2007-81. **Mentzen, B.F.** *Crystallographic Determination of the Positions of the Monovalent H, Li, Na, K, Rb, and Tl Cations in Fully Dehydrated MFI Type Zeolites*
J. Phys. Chem. C, **111**,51, 18932 -18941, 2007

2007-82. **Mentzen, B.F., Bergeret, G.** *Crystallographic Determination of the Positions of the Copper Cations in Zeolite MFI*
J. Phys. Chem. C, **111**, 34, 12512 -12516, 2007

2007-83. **Mørkved, E.H., Beukes, J.A., Mo, F.** *-Quinonoid Heterocycles: Synthesis and Crystal Structure of 2,3-Dicyano-5,7-bismethylthieno[3,4-b]pyrazine*
Molecules, **12**, 1623-1631, 2007

2007-84. **Nilsen, M.H., Antonakou, E., Bouzga, A., Lappas, A., Mathisen, K., Stöcker, M.** *Investigation of the effect of metal sites in Me–Al-MCM-41 (Me = Fe, Cu or Zn) on the catalytic behavior during the pyrolysis of wooden based biomass*
Microp. & Mesop. Mat., **105**, 1-2, 189-203, 2007

2007-85. **Nilsen, M., Nordhei, C., Ramstad, A.L., Nicholson, D., Poliakoff, M., Cabañas, A.** *XAS (XANES and EXAFS) investigations of Nanoparticulate Ferrites synthesized continuously in near critical and supercritical water*
J. Phys. Chem. C, **111**, 17, 6252 - 6262, 2007

2007-86. **Oksanen, E., Ahonen, A.-K., Tuominen, H., Tuominen, V., Lahti, R., Goldman, A., Heikinheimo, P.** *A complete structural description of the catalytic cycle of Yeast Pyrophosphatase*
Biochemistry, **46**, 5, 1228 -1239, 2007

2007-87. **Oliéric, V., Ennifar, E., Meents, A., Fleurant, M., Besnard, C., Pattison, P., Schiltz, M. et al.** *Using X-ray absorption spectra to monitor specific radiation damage to anomalously scattering atoms in macromolecular crystallography*
Acta Cryst., D**63**, 759-768, 2007

2007-88. **Opalka, S.M., Lvvik, O.M., Brinks, H.W., Saxe, P.W., Hauback, B.C.** *Integrated experimental-theoretical investigation of the Na-Li-Al-H system*
Inorg. Chem., **46,** 4, 1401 - 1409, 2007

2007-89. **Palin, L., Brunelli, M., Pattison, Ph., Fitch, A.N.** *A structural investigation of the four phases of 7-oxabicyclo [2.2.1] heptane*
Z. Kristallographie, **222**, 9, 487-491, 2007

2007-90. **Pastore, H., De Oliveira, E., Superti, G., Gatti, G., Marchese, L.** *Reaction at interfaces: the silicoaluminophosphate molecular sieve CAL-1*
J. Phys. Chem. C, **111**, 3116-3129, 2007

2007-91. **Pouchon, M.A., Chen, J.C., Degueldre, C., Froideval, A., Emerich, H., Van Beek, W.** *EXAFS Study on Irradiated ODS Ferritic Steel PRICM 6*
Materials Science Forum, **561**, 1761-1764, 2007

2007-92. **Rabe, S., Nachtegaal, M., Vogel, F.** *Catalytic partial oxidation of methane to synthesis gas over a ruthenium catalyst: the role of the oxidation state*
Phys. Chem. Chem. Phys., **9**, 1461 - 1468, 2007

2007-93. **Renaudin, G., Mapemba, E., El-Ghozzi, M., Dubois, M., Avignant, D., Cerný, R.** *Combined high resolution powder and single-crystal diffraction to determine the structure of* $Li_{1+x}Ce^{III}_{x}Ce^{IV}_{6-x}F_{25}$
Z. Kristallog., **Suppl.26**, 455-460, 2007

2007-94. **Rieder, M., Crelling, J.C., Šustai,O., Drábek, M., Weiss, Z., Klementová, M.** *Arsenic in iron disulfides in a brown coal from the North Bohemian Basin, Czech Republic*
Int. J. Coal Geology , **71**, 2-3, 115-121, 2007

2007-95. **Riise, E.K., Lorentzen, M.S., Helland, R., Smalås, A.O., Leiros, H.-K.S., Willassen, N.P.** *The first structure of a cold-active catalase from Vibrio salmonicida at 1.96 Å reveals structural aspects of cold adaptation*
Acta Cryst., D**63**, 135-148, 2007

2007-96. **Riktor, M. D., Sørby, M. H., Chopek, K., Fichtner, M., Buchter, F., Züttel, A., Hauback, B. C.** *In situ synchrotron diffraction studies of phase transitions and thermal decomposition of* $Mg(BH_4)_2$ *and* $Ca(BH_4)_2$
J. Mater. Chem., **17,** 4939 - 4942, 2007

2007-97. **Sanishvili, R., Besnard, C., Camus, F., Fleurant, M., Pattison, P., Bricogne, G., Schiltz, M.** *Polarization-dependence of anomalous scattering in brominated DNA and RNA molecules, and importance of crystal orientation in single- and multiple-wavelength anomalous diffraction phasing*
J. Appl. Cryst., **40**, 552-558, 2007

2007-98. **Schaub, P., Weber, T., Steurer, W.** *Exploring local disorder in single crystals by means of the three-dimensional pair distribution function*
Philosophical Mag., **87**, 2781 - 2787 , 2007

2007-99. **Serre, Ch., Bourrelly, S., Vimont, A., Ramsahye, N., Maurin, G., Llewellyn, Ph., Daturi, M., Filinchuk, Y. et al.** *An explanation for the very large breathing effect of a metal-organic framework during* CO_2 *absorption*
Adv. Materials, **19**, 17, 2246-2251, 2007

2007-100. **Serre, C., Mellot-Draznieks, C., Surblé, S., Audebrand, N., Filinchuk, Y., Férey, G.** *Role of solvent-host interactions that lead to very large swelling of hybrid frameworks* Science, **315**, 5820, 1828 - 1831, 2007

2007-101. **Siegrist, T., Besnard, C., Haas, S., Schiltz, M., Pattison, P., Chernyshov, D., Batlogg, B., Kloc, C.** *A Polymorph Lost and Found: The High-Temperature Crystal Structure of Pentacene*
Adv. Materials, **19,** 16, 2078-2082, 2007

2007-102. **Sikorski, P., Mo, F., Skjåk-Bræk, G., Stokke, B.T.** *Evidence for Egg-Box-Compatible Interactions in Calcium-Alginate Gels from Fiber X-ray Diffraction*
Biomacromolecules, **8,** 7, 2098 -2103, 2007

2007-103. **Sørby, M.H., Nakamura, Y., Brinks, H.W., Ichikawa, T., Hino, S., Fujii, S., Hauback, B.C.** *The crystal structure of* $LiND_2$ *and* $Mg(ND_2)_2$
J. Alloys & Compounds, **428**, 1-2 , 297-301, 2007

2007-104. **Van der Maelen, J. F., Gutiérrez-Puebla, E., Monge, Á., García-Granda, S., Resa, I., Carmona, E., Fernández-Díaz, M. T., McIntyre, G. J., Pattison, P., Weber, H.-P.** *Experimental and theoretical characterization of the Zn-Zn bond in* $[Zn_2(\cdot 2\text{-}C_5Me_5)_2]$
Acta Cryst., B**63**, 862-868, 2007

2007-105. **Van Mechelen, J. B., Peschar, R., Schenk, H.** *The crystal structures of the ß1 and ß2 polymorphs of mono-unsaturated triacylglycerols and cocoa butter determined from high resolution powder diffraction data*
Z. Kristallogr. **Suppl. 26**, 599-604, 2007

2007-106. **Vespa, M., Dähn, R., Grolimund, D., Wieland, E., Scheidegger, A. M.** *Co speciation in hardened cement paste: a macro- and micro-spectroscopic investigation*
Environ. Sci. Technol., **41**, 6, 1902 -1908, 2007

2007-107. **Vespa, M., Wieland, E., Dähn, R., Grolimund, D., Scheidegger, A.M.** *Determination of the elemental distribution and chemical speciation in highly heterogeneous cementitious materials using synchrotron-based micro-spectroscopic techniques*
Cement & Concrete Res., **37**, 11, 1473-1482 , 2007

2007-108. **Vrålstad, T., Øye, G., Stöcker, M., Sjöblom, J.** *Synthesis of comparable Co-MCM-48 and Co-MCM-41 materials containing high cobalt contents*
Microp. & Mesop. Mater., **104**, 1-3, 10-17, 2007

2007-109. **Weiher N., Beesley A.M., Tsapatsaris N., Louis C., Delannoy L., Van Bokhoven J.A., Schroeder S.L.M.** I*n situ XAS studies on the structure of the active site of supported gold catalysts*
AIP Conference Proceedings **882**, 600-602, 2007 In: "X-RAY ABSORPTION FINE STRUCTURE - XAFS13: 13th International Conference" - Stanford, California,USA

2007-110. **Yartys, V.A., Denys, R.V., Maehlen, J.P., Frommen, Ch., Fichtner, M., Bulychev, B.M., Emerich, H.** *Double-Bridge Bonding of Aluminium and Hydrogen in the Crystal Structure of gamma-AlH_3*
Inorg. Chem., **46**, 4, 1051 - 1055, 2007

2007-111. **Yvon, K., Rapin, J.-Ph., Penin, N., Ma, Zhu, Chou, M.Y.** *LaMg2PdH7, a new complex metal hydride containing tetrahedral $[PdH_4]^{4-}$ anions*
J. Alloys & Compounds, **446-447**, 34-38, 2007

2007-112. **Zanardi, S., Cruciani, G., Carluccio, L.C., Bellussi, G., Perego, C., Millini, R.** *Synthesis and framework topology of the new disordered ERS-10 zeolite*
J. Porous Mater.,**14**, 3 , 315-323, 2007

2008

2008-1. **Albertsen, J., Grong, Ø., Walmsley, J., Mathiesen, R., Van Beek, W.** *A Model for High-Temperature Pitting Corrosion in Nickel-Based Alloys Involving Internal Precipitation of Carbides, Oxides, and Graphite*
Metallur. & Mater. Transac. A, **39A**, 6, 1258-1276, 2008

2008-2. **Arakcheeva, A., Pattison, P., Chapuis, G., Rossell, M., Filaretov, A. et al.** *$KSm(MoO_4)_2$, an incommensurately modulated and partially disordered scheelite-like structur*e
Acta Cryst., B**64**, 160-171, 2008

2008-3. **Baerlocher, Ch., Xie, D., McCusker, L., Hwang, S.-J., Chan, I., Ong, K. et al.** *Zones Ordered silicon vacancies in the framework structure of the zeolite catalyst SSZ-74*
Nature Materials, in press, 2008

2008-4. **Blanchard, D., Lem, A., Øvergaard, S., Brinks, H., Hauback, B.** *$LiAlD_4$ with VCl_3 additives: influence of ball-milling energies*
J. Alloys & Compounds, **458**, 1-2, 467-473, 2008

2008-5. **Boldyreva, E., Sowa, H., Ahsbahs, H., Goryainov, S., Chernyshev, D., Dmitriev, V. et al.** *Pressure-induced phase transitions in organic molecular crystals: a combination of x-ray single-crystal and powder diffraction, raman and IR-spectroscopy*
J. Phys.: Conf. Ser. **121**, 022023 , 2008

2008-6. **Borodi, G., Bratu, I., Dragan, F., Peschar, R., Helmholdt, R.B., Hernanz, A.** *Spectroscopic investigations and crystal structure from synchrotron powder data of the inclusion complex of ß-cyclodextrin with atenolol Spectrochim*
Acta Part A: Mol. Biomol. Spectrosc., **70**, 1041-1048, 2008

2008-7. **Bosak, A., Chernyshov, D.** *Model-free reconstruction of lattice dynamics from thermal diffuse scattering*
Acta Cryst., A **64**, 598-600, 2008

2008-8. **Brinks, H., Fossdal, A., Hauback, B.** *Adjustment of the Stability of Complex Hydrides by Anion Substitution*
J. Phys. Chem., C **112**, 14, 5658 -5661, 2008

2008-9. **Brodski, V., Peschar, R., Schenk, H., Brinkmann, A., Van Eck, E., Kentgens, A.** *Structure of Tetrakis(melaminium) Bis(dihydrogenphosphate) Monohydrogenphosphate Trihydrate from X-ray Powder Diffraction and Solid-State NMR Spectroscopy*
J. Phys. Chem. C, **112**, 32, 12515–12523, 2008

2008-10. **Buchter, F., Lodziana, Z., Remhof, A., Friedrichs, O., Borgschulte, A. et al**. *Structure of $Ca(BD_4)_2$ beta-Phase from Combined Neutron and Synchrotron X-ray Powder Diffraction Data and Density Functional Calculations*
J. Phys. Chem. B, **112**, 27, 8042–8048, 2008

2008-11. **Casapu, M., Grunwaldt, J.-D., Maciejewski, M., Krumeich, F., Baiker, A. et al.** *Comparative study of structural properties and NO_x storage-reduction behavior of $Pt/Ba/CeO_2$ and $Pt/Ba/Al_2O_3$*
Appl. Catalysis B: Environmental, **78**, 3-4, 288-300, 2008

2008-12. **Chen, X.-Y., Marchal, C., Filinchuk, Y., Imbert, D., Mazzanti, M.** *A flexible tripodal ligand linking octametallic terbium rings into luminescent polymeric chains*
Chem. Commun., 3378 - 3380, 2008

2008-13. **Chernyshov, D., Dmitriev, V., Pomjakushina, E., Conder, K., Stingaciu, M. et al.** *Superstructure formation at the metal-insulator transition in $RBaCo_2O_{5.5}$ (R=Nd,Tb) as seen from reciprocal space mapping*
Phys. Rev., B **78**, 024105-024112, 2008

2008-14. **Crosignani, S., Page, P., Missotten, M., Colovray, V., Cleva, Ch. et al.** *Discovery of a New Class of Potent, Selective, and Orally Bioavailable CRTH2 (DP2) Receptor Antagonists for the Treatment of Allergic Inflammatory Diseases#*
J. Med. Chem., **51**, 7, 2227–2243, 2008

2008-15. **Denys, R.V., Riabov, A.B., Yartys, V.A., Sato, M., Delaplane, R.G**. *Mg substitution effect on the hydrogenation behaviour, thermodynamic and structural properties of the La_2Ni_7–$H(D)_2$ system*
J. Solid State Chem., **181**, 4, 812-821, 2008

2008-16. **Dietzel, P. D. C., Johnsen, R. E., Blom, R., Fjellvåg, H.** *Structural Changes and Coordinatively Unsaturated Metal Atoms on Dehydration of Honeycomb Analogous Microporous Metal-Organic Frameworks*
Chem. - A Eur. J., **14**, 8, 2389 - 2397, 2008

2008-17. **Dmitriev, V., Filinchuk, Y., Chernyshov, D., Talyzin, A.V., Dzwilevski, A. et al.** *Pressure-temperature phase diagram of $LiBH_4$: Synchrotron x-ray diffraction experiments and theoretical analysis*
Phys. Rev. B **77**, 174112-174123, 2008

2008-18. **Dondi, M., Matteucci, F., Baldi, D., Barzanti, A., Cruciani, G., Zama, I., Bianchi, C.L.** *Gray–blue Al_2O_3–MoO_x ceramic pigments: Crystal structure, colouring mechanism and performance*
Dyes & Pigments , **76**, 1, 179-186, 2008

2008-19. **Dubarry, M., Gaubicher, J., Guyomard, D., Wallez, G., Quarton, M., Baehtz, C**. *Uncommon potential hysteresis in the $Li/Li_{2x}VO(H_{2-x}PO_4)_2$ ($0 \leq x \leq 2$) system*
Electrochimica Acta, **53**, 13, 4564-4572, 2008

2008-20. **Filinchuk, Y., Chernyshov, D., Cerny, R.** *Lightest Borohydride Probed by Synchrotron X-ray Diffraction: Experiment Calls for a New Theoretical Revision*
J. Phys. Chem. C, **112**, 28, 10579–10584, 2008

2008-21. **Filinchuk, Y., Chernyshov, D., Nevidomskyy, A., Dmitriev, V.** *High-Pressure Polymorphism as a Step towards Destabilization of $LiBH_4$*
Angew. Chem. Int. Ed., **47**, 3, 529 - 532, 2008

2008-22. **Filinchuk, Y., Hagemann, H.** *Structure and Properties of $NaBH_4 \cdot 2H_2O$ and $NaBH_4$*
Eur. J. Inorg. Chem., **20**, 3127 - 3133, 2008

2008-23. **Filinchuk, Y., Lisnyak, V.V., Stratiichuk, D.A., Stus, N.V.** *Crystal structure of $Nax(MoO)_5(P_2O_7)_4$ studied by synchrotron X-ray diffraction*
J. Alloys & Compounds, **463**, 1-2, 124-128, 2008

2008-24. **Fois, E., Gamba, A., Medici, C., Tabacchi, G., Quartieri, S., Mazzucato, E., Arletti, R., Vezzalini, G., Dmitriev, V.** *High pressure deformation mechanism of Li-ABW: Synchrotron XRPD study and ab initio molecular dynamics simulations*
Microp. & Mesop. Mat., **115**, 267-280, 2008

2008-25. **Galli, E., Gualtieri, A.F.** *Direnzoite, [$NaK_6MgCa_2(Al_{13}Si_{47}O_{120})\cdot 36H_2O$], a new zeolite from Massif Central (France): Description and crystal structure*
Am. Mineralogist, **93**, 95-102, 2008

2008-26. **Gao, T., Glerup, M., Krumeich, F., Nesper, R., Fjellvåg, H., Norby, P.** *Microstructures and Spectroscopic Properties of Cryptomelane-type Manganese Dioxide Nanofibers*
J. Phys. Chem. C, **112,** 34, 13134–13140, 2008

2008-27. **Grove, H., Brinks, H., Heyn, R., Wu, F.-J., Opalka, S. et al.** *The structure of $LiMg(AlD_4)_3$*
J. Alloys & Compounds, **455**, 1-2, 249-254, 2008

2008-28. **Grove, H., Brinks, H., Løvvik, O., Heyn, R., Hauback, B.** *The crystal structure of $LiMgAlD_6$ from combined neutron and synchrotron X-ray powder diffraction*
J. Alloys & Compounds, **460**, 1-2, 64-68, 2008

2008-29. **Gualtieri, A., Ferrari, S., Leoni, M., Grathoff, G., Hugo, R. et al.** *Structural characterization of the clay mineral illite-1M*
Applied Crystal., **41**, 2, 402-415, 2008

2008-30. **Hagemann, H., Longhini, M., Kaminski, J., Wesolowski, T. et al.** *$LiSc(BH_4)_4$: A Novel Salt of Li+ and Discrete $Sc(BH_4)_4$ - Complex Anions*
J. Phys. Chem. A, **112**, 33, 7551–7555, 2008

2008-31. **Hamacek, J., Bernardinelli, G., Filinchuk, Y.** *Tetrahedral Assembly with Lanthanides: Toward Discrete Polynuclear Complexes*
Eur. J. Inorg. Chem., **22**, 3419 - 3422, 2008

2008-32. **Helland, R., Fjellbirkeland, A., Karlsen, O., Ve, Th., Lillehaug, J., Jensen, H.** *An Oxidized Tryptophan Facilitates Copper Binding in Methylococcus capsulatus-secreted Protein MopE**
J. Biol. Chem., **283**, 20, 13897-13904, 2008

2008-33. **Hersleth, H.-P., Hsiao, Y.-W., Ryde, U., Gorbitz, C.H., Andersson, K.** *The crystal structure of peroxymyoglobin generated through cryoradiolytic reduction of myoglobin compound III during data collection*
Biochem. J., **412**, 257–264, 2008

2008-34. **Hersleth, H.-P., Varnier, A., Harbitz, E., Røhr, Å., Schmidt, P., Sørlie, M. et al.** *Reactive complexes in myoglobin and nitric oxide synthase Inorganica*
Chimica Acta, **361**, 4, 831-843, 2008

2008-35. **Horcajada, P., Serre, Ch., Maurin, G., Ramsahye, N., Balas, F., Vallet-Regí, M. et al.** *Flexible Porous Metal-Organic Frameworks for a Controlled Drug Delivery*
J. Am. Chem. Soc., **130**, 21, 6774–6780, 2008

2008-36. **Huber, F., Venvik, H., Rønning, M. Walmsley, J., Holmen, A.** *Preparation and characterization of nanocrystalline, high-surface area CuCeZr mixed oxide catalysts from homogeneous co-precipitation* Chem. Eng. J., **137**, 3, 686-702, 2008

2008-37. **Hušák, M., Jegorov, A., Brus, J., Van Beek, W., Pattison, P. et al.** *Metergoline II: structure solution from powder diffraction data with preferred orientation and from microcrystal*
Struct. Chem., **19**, 3, 512-525, 2008

2008-38. **Kiebach, R., Pienack, N., Bensch, W., Grunwaldt, J.-D. et al.** *Hydrothermal Formation of W/Mo-Oxides: A Multidisciplinary Study of Growth and Shape*
Chem. Mater., **20**, 9, 3022–3033, 2008

2008-39. **Kowalchuk, C., Paz, F., Ananias, D., Pattison, Ph., Carlos, L., Rocha, J.** *Photoluminescent Microporous Lanthanide Silicate AV-21 Frameworks*
Chem. - A Eur. J., in press, 2008

2008-40. **Lambert, J., Wallez, G., Quarton, M., Le Mercier, T., Van Beek, W.** *Searching for the dopant ion in Eu^{2+}-activated $BaMgAl_{10}O_{17}$ phosphor with synchrotron diffraction*
J. Luminescence, **128**, 366-372, 2008

2008-41. **Llewellyn, Ph., Maurin, G., Devic, Th., Loera-Serna, S., Rosenbach, N. et al.** *Prediction of the Conditions for Breathing of Metal Organic Framework Materials Using a Combination of X-ray Powder Diffraction, Microcalorimetry, and Molecular Simulation*
J. Am. Chem. Soc., in press, 2008

2008-42. **Mantion, A., Massüger, L., Rabu, P., Palivan, C., McCusker, L., Taubert, A.** *Metal-Peptide Frameworks (MPFs): "Bioinspired" Metal Organic Frameworks*
J. Am. Chem. Soc., **130**, 8, 2517-2526, 2008

2008-43. **Millange, F., Serre, Ch., Guillou, N., Férey, G., Walton, R.I.** *Structural Effects of Solvents on the Breathing of Metal-Organic Frameworks: An In Situ Diffraction Study*
Angew. Chem. Int. Ed., **47**, 22 , 4100 - 4105, 2008

2008-44. **Nakamura, Y., Hino, S., Ichikawa, T., Fujii, H., Brinks, H., Hauback, B.** *Dehydrogenation reaction of Li-Mg-N-H systems studied by in situ synchrotron powder X-ray diffraction and powder neutron diffraction*
J. Alloys & Compounds, **457**, 1-2, 362-367, 2008

2008-45. **Nielsen, R., Kongshaug, K., Fjellvåg, H.** *Delamination, synthesis, crystal structure and thermal properties of the layered metal-organic compound $Zn(C_{12}H_{14}O_4)$*
J. Mater. Chem., 2008, **18**, 1002 - 1007

2008-46. **Nordhei, C., Ramstad, A., Nicholson, D.** *Nanophase cobalt, nickel and zinc ferrites: synchrotron XAS study on the crystallite size dependence of metal distribution*
Phys. Chem. Chem. Phys., **10**, 1053-1066, 2008

2008-47. **Ori, S., Quartieri, S., Vezzalini, G., Dmitriev, V.** *Pressure-induced structural deformation and elastic behavior of wairakite*
Am. Mineralogist, **93**, 53-62, 2008

2008-48. **Palacios, L., Cabeza, A., Bruque, S., García-Granda, S., Aranda, M.** *Structure and Electrons in Mayenite*
Electrides Inorg. Chem., **47**, 7, 2661–2667, 2008

2008-49. **Pillet, S., Legrand, V., Weber, H.-P., Souhassou, M., Létard, J.-F., Guionneau, Ph., Lecomte, C.** *Out-of-equilibrium charge density distribution of spin crossover complexes from steady-state photocrystallographic measurements: experimental methodology and results*
Z. Kristallogr., **223**, 4-5, 235-249, 2008

2008-50. **Pitt, M., Vullum, P., Sørby, M., Sulicc, M., Jensen, C. et al.** *Structural properties of the nanoscopic Al_{85} Ti_{15} solid solution observed in the hydrogen-cycled $NaAlH_4$ + 0.1$TiCl_3$ system*
Acta Materialia, in press, 2008

2008-51. **Renaudin, G., Laquerrière, P., Filinchuk, Y., Jallot, E., Nedelec, J.M**. *Structural characterization of sol–gel derived Sr-substituted calcium phosphates with anti-osteoporotic and anti-inflammatory properties*
J. Mater. Chem., **18**, 3593 - 3600, 2008

2008-52. **Remmerie, B., Vandenbroucke, K., De Smet, L., Carpentier, W. et al.** *Expression, purification, crystallization and structure determination of two glutathione S-transferase-like proteins from Shewanella oneidensis*
Acta Cryst., F **64**, 6, 548-553, 2008

2008-53. **Rouquette, J., Kantor, I., McCammon, C., Dmitriev, V., Dubrovinsky, L.** *High-Pressure Studies of $(Mg_{0.9}Fe_{0.1})2SiO_4$Olivine Using Raman Spectroscopy, X-ray Diffraction, and Mössbauer Spectroscopy*
Inorg. Chem., **47**, 7, 2661–2667, 2008

2008-54. **Sartori, S., Opalka, S., Løvvik, O., Guzik, M., Tang, X., Hauback, B.** *Experimental studies of alpha-AlD_3 and alpha'-AlD_3 versus first-principles modelling of the alane isomorphs*
J. Mater. Chem., **18**, 2361 - 2370, 2008

2008-55. **Schiltz, M., Bricogne, G.** *Exploiting the anisotropy of anomalous scattering boosts the phasing power of SAD and MAD experiments*
Acta Cryst., D **64**, 7, 711-729, 2008

2008-56. **Sereda, O., Neels, A., Stoeckli, F., Stoeckli-Evans, H., Filinchuk, Y.** *Sponge-like Reversible Transformation of a Bimetallic Cyanometallate Polymer*
Cryst. Growth Des., **8**, 7, 2307–2311, 2008

2008-57. **Serre, C., Surblé, S., Mellot-Draznieks, C., Filinchuk, Y., Férey, G.** *Evidence of flexibility in the nanoporous iron(III) carboxylate MIL-89*
Dalton Trans., in press, 2008

2008-58. **Talysin, A., Solozhenko, V., Kurakevych, O., Szabo, T., Dekany, I., Kurnosov, A., Dmitriev, V.** *Pressure-Induced Lattice Expansion of Graphite Oxide in the Presence of Water*
Angewandte Chem. Int. Ed, **47**, in press, 2008

2008-59. **Tokaychuk, Y., Filinchuk, Y., Sheptyakov, D., Yvon, K.** *Hydrogen Absorption in Transition Metal Silicides: La3Pd5Si-Hydrogen System*
Inorg. Chem., in press, 2008

2008-60. **Tonti, D., Mohammed, M., Al-Salman, A., Pattison, Ph., Chergui, M**. *Multimodal Distribution of Quantum Confinement in Ripened CdSe Nanocrystals*
Chem. Mater., **20**, 4, 1331–1339, 2008

2008-61. **Van Mechelen, J., Peschar, R., Schenk, H.** *Structures of mono-unsaturated triacylglycerols. III. The beta-2 polymorphs of trans-mono-unsaturated triacylglycerols and related fully saturated triacylglycerols*
Acta Cryst., B **64**, 240-248, 2008

2008-62. **Van Mechelen, J., Peschar, R., Schenk, H.** *Structures of mono-unsaturated triacylglycerols. IV. The highest melting beta'-2 polymorphs of trans-mono-unsaturated triacylglycerols and related saturated TAGs and their polymorphic stability*
Acta Cryst., B **64**, 249-259, 2008

2008-63. **Veen, S., Roy, S., Filinchuk, Y., Chernyshov, D., Petukhov, A. et al.** *Extended Structure Design with Simple Molybdenum Oxide Building Blocks and Urea As a Directing Agent*
Inorg. Chem., **47**, 15, 6863–6866, 2008

2008-64. **Vorobiev, A., Chernyshov, D., Godeev, G., Orlova, D.** *Non-destructive characterization of ferrofluids by wide-angle synchrotron light diffraction: crystalline structure and size distribution of colloidal nanoparticles*
Acta Cryst. C, in press, 2008

2008-65. **Winne, J., De Clercq, P., Milanesio, M., Pattison, Ph., Viterbo, D**. *Nonenzymic polycyclisation of analogues of oxidosqualene with a preformed C-ring*
Org. Biomol. Chem., 2008, **6**, 1918 - 1925

2008-66. **Wieland, E., Tits, J., Kunz, D., Dähn, R.** *Strontium Uptake by Cementitious*
Materials Environ. Sci. Technol., **42**, 2, 403–409, 2008

2008-67. **Wright, J., Besnard, C., Margiolaki, I., Basso, S., Camus, F., Fitch, F. et al.** *Molecular envelopes derived from protein powder diffraction data*
J.Appl.Cryst., **41**, 329-339, 2008

2008-68. **Yu, Zh., Chen, D., Rønning, M., Vrålstad, T., Ochoa-Fernández, E., Holmen, A.** *Large-scale synthesis of carbon nanofibers on Ni–Fe–Al hydrotalcite derived catalysts I. Preparation and characterization of the Ni–Fe–Al hydrotalcites and their derived catalysts*
Appl. Catalysis A: General, **338,** 1-2, 136-146, 2008

2008-69. **Yu, Zh., Chen, D., Rønning, M., Vrålstad, T., Ochoa-Fernández, E., Holmen, A.** *Large-scale synthesis of carbon nanofibers on Ni-Fe-Al hydrotalcite derived catalysts II: Effect of Ni/Fe composition on CNF synthesis from ethylene and carbon monoxide*
Appl. Catalysis A: General, **338**, 1-2, 147-158, 2008

2008-70. **Zaharko, O., Mesot, J., Salguero, L., Valentí R., Zbiri, M., Johnson, M., Filinchuk, Y. et al.** *Tetrahedra system $Cu_4OCl_6daca_4$: High-temperature manifold of molecular configurations governing low-temperature properties*
Phys. Rev. B **77**, 224408-224419, 2008

PhD Theses
(based in part on data from SNBL)

Albertsen J.Z.
NTNU Trondheim (Norway), 2007
Experimental and theoretical investigations of metal dusting corrosion in plant exposed nickel-based alloys.

Borg Ø.
NTNU, Trondheim (Norway), 2007
Role of Alumina Support in Cobalt Fischer-Tropsch Synthesis.

Bus E.
ETH Zürich (Switzerland), 2007
Characterization of supported gold, platinum-gold, and platinum catalysts for hydrogenation reactions.

Gramm F.
ETH Zürich (Switzerland), 2007
Kombination von Transmissionselektronenmikroskopie und Pulverbeugungsdaten zur Losung von komplexen Zeolithstrukturen.

Hersleth, H.-P.
University of Oslo (Norway), 2007
Strutural studies of hydrogen peroxide derived myoglobin complexes.

Nordhei C.
NTNU Trondheim (Norway), 2008
Aspects of electronic and structural properties of nanophase cubic ferrites studied by X-ray absorption spectroscopy.

Van Mechelen J.B.
Universiteit van Amsterdam (The Netherlands), 2008
Triacylglycerol structures and the chocolate fat bloom mechanism. A high resolution powder diffraction study.